Using satellite data to improve the leaf phenology of a global Terrestrial Biosphere Model

N. MacBean[1], F. Maignan[2], P. Peylin[1], C. Bacour[2], F.-M. Bréon[1], P. Ciais[1]

[1]{Laboratoire des Sciences du Climat et de l'Environnement, Gif sur Yvette Cedex, 91191, France}

[2]{NOVELTIS, Labège, France}

Correspondence to: N. MacBean (nlmacbean@gmail.com)

Abstract

Correct representation of seasonal leaf dynamics is crucial for Terrestrial Biosphere Models (TBMs), but many such models cannot accurately reproduce observations of leaf onset and senescence. Here we optimized the phenology-related parameters of the ORCHIDEE TBM using satellite-derived Normalized Difference Vegetation Index data (MODIS NDVI v5) that are linearly related to the model fAPAR. We found the misfit between the observations and the model decreased after optimisation for all boreal and temperate deciduous Plant Functional Types, primarily due to an earlier onset of leaf senescence. The model bias was only partially reduced for tropical deciduous trees and no improvement was seen for natural C4 grasses. Spatial validation demonstrated the generality of the posterior parameters for use in global simulations, with an increase in global median correlation of 0.56 to 0.67. The simulated global mean annual Gross Primary Productivity decreased by ~10PgCyr^{-1} over the 1990-2010 period due to the substantially shortened Growing Season Length (GSL – by up to 30 days in the Northern Hemisphere), thus reducing the positive bias and improving the seasonal dynamics of ORCHIDEE compared to independent data-based estimates. Finally, the optimisations led to changes in the strength and location of the trends in the simulated vegetation productivity as represented by the GSL and mean annual fraction of Absorbed Photosynthetically Active Radiation (fAPAR), suggesting care should be taken when using un-calibrated models in attribution studies. We suggest that the framework presented here can be applied for improving the phenology of all global TBMs.

Natasha MacBean 5/11/2015 10:58
Deleted: GSL and mean annual fAPAR

1   Introduction

Leaf phenology, the timing of leaf onset, growth and senescence, is a critical component of the coupled soil-vegetation-atmosphere system as it directly controls the seasonal exchanges of carbon, C, as well as affecting the surface energy balance and hydrology through changing albedo, surface roughness, soil moisture and evapotranspiration. In turn leaf phenology is largely governed by the climate, as leaf onset and senescence are triggered by seasonal changes in temperature, moisture and radiation. Leaf phenology is therefore sensitive to inter-annual climate variability and future climate change (Cleland et al., 2007; Körner and Basler, 2010; Reyer et al., 2013), as well as to increasing atmospheric CO_2 concentrations (Reyes-Fox et al., 2014), and will feedback on both (Richardson et al., 2013). It is expected that climate warming will advance leaf onset in temperature limited northern biomes. Such trends have already been observed in the northern hemisphere (NH) using either satellite or in-situ observations (Badeck et al., 2004; Delbart et al., 2008; Jeong et al., 2011; Myneni et al., 1997; Parmesan, 2007). However, increasing temperatures may either advance or delay senescence, depending on species-specific responses to other environmental variables (Hänninen and Tanino, 2011; Piao et al., 2007). Future changes of precipitation in a warming climate will also likely affect tropical and semi-arid ecosystems that are more controlled by moisture availability (e.g. Anyamba and Tucker, 2005; Dardel et al., 2014; Fensholt et al., 2012).

In order to improve predictions of the impact of future climate change on vegetation and its interaction with the global C and water cycles, it is crucial to have prognostic leaf phenology schemes in process-based Terrestrial Biosphere Models (TBMs) that constitute the land component of Earth System Models (ESMs) (Kovalskyy and Henebry, 2012b; Levis and Bonan, 2004). Many such models exist in the literature, especially for temperate and boreal forests (e.g. Arora and Boer, 2005; Caldararu et al., 2014; Chuine, 2000; Hänninen and Kramer, 2007; Knorr et al., 2010; Kovalskyy and Henebry, 2012a) and have been included in most TBMs. However, model evaluation studies have shown that there are biases in the growing season length and magnitude of the leaf area index (LAI) predicted by TBMs when compared to ground-based observations of leaf emergence and LAI (Kucharik et al., 2006; Richardson et al., 2012) or satellite-derived measures of vegetation greenness and LAI (Kim and Wang, 2005; Lafont et al., 2012; Maignan et al., 2011; Murray-Tortarolo et al., 2013). This can result in systematic errors in model predictions of the seasonal carbon, water and energy exchanges (Kucharik et al., 2006; Richardson et al., 2012; Walker et al., 2014).

As is always the case prior to model parameter calibration, it is unclear whether the misfit between modelled and observed measures of leaf phenology is the result of inaccurate parameter values, model structural error, or both. In order to answer this question, the parameters first need to be optimized using Data Assimilation (DA) techniques, and if the models cannot reproduce the data within defined uncertainties we expect to gain insights into possible directions for model improvement. DA is also a useful way to better characterize and possibly reduce uncertainty in model simulations, and to determine the relative influence of parametric, structural and driver uncertainty (e.g. Migliavacca et al., 2012).

Many studies have optimized the parameters of phenology models for a range of species with ground-based observations of the date of leaf onset (Blümel and Chmielewski, 2012; Chuine et al., 1998; Fu et al., 2012; Jeong et al., 2012), the "green fraction" derived from ground-based digital photography (Migliavacca et al., 2011) or with spring onset dates derived from carbon fluxes taken at flux tower sites (Melaas et al., 2013). Melaas et al. (2013) went further and demonstrated the transferability of parameters in time and between sites by including multiple sites in the optimisation. All of these studies have used DA to test different phenology model structures, thereby contributing significantly to the debate about whether a simple classical temperature-driven budburst model is sufficient, or whether more complex chilling and/or photoperiodic cues are needed to best predict leaf onset. Several studies also investigated the impacts of optimizing phenology on the resulting C and water budgets (Migliavacca et al., 2012; Picard et al., 2005, Richardson and O'Keefe, 2009).

Peñuelas et al. (2009) noted that medium- to coarse-resolution satellite data might be more appropriate for optimizing the phenology in TBMs, due to the large difference in scale between the resolution of a typical model grid cell ($1x1^{o}$) and ground-based data, which may cause representation errors (Rayner, 2010). A few studies to date have performed a global optimisation of model phenology using satellite data, in the sense that multiple sites and/or Plant Functional Types (PFTs) are included in the assimilation (Forkel et al., 2014; Knorr et al., 2010; Stöckli et al., 2011). In this study we aim to reinforce this line of research and to answer the following questions:

i) Can we constrain the phenology-related parameters and processes of a typical process-based TBM at global scale using satellite "greenness" index data?

ii) Does this produce a generic parameter set that results in improved simulations of the seasonal cycle of the vegetation, or are further model structural developments required?

iii) What is the impact of the optimisation on mean patterns and trends in vegetation productivity (as represented by the mean fraction of Absorbed Photosynthetically Active Radiation (fAPAR), amplitude and Growing Season Length (GSL)) at regional and global scales?

To achieve this we performed a global, multi-PFT, multi-site optimisation of the phenology model parameters for the six non-agricultural deciduous PFTs of the ORCHIDEE TBM. The phenology models in ORCHIDEE are common to many process-based TBMs. Note there is no specific phenology model associated to evergreen PFTs, where leaf turnover is simply a function of climate and leaf age.

Some of the carbon cycle-related parameters of ORCHIDEE (including phenology-related parameters) have previously been optimized using in situ flux measurements (e.g. Kuppel et al., 2014; Santaren et al., 2014; Bacour et al., 2015). Here we focus purely on improving the *timing* of both spring onset and autumn senescence of ORCHIDEE at global scale, by using a novel approach to assimilate normalized medium-resolution satellite-derived vegetation "greenness" index data (MODIS NDVI collection 5) that are linearly related to the simulated daily fAPAR. The aim of a multi-site (MS) (i.e. model grid cell) assimilation is to find a unique parameter set for each PFT that results in a similar improvement as a single-site (SS) optimisation, as the range of posterior parameter values for individual sites/species can be large (Richardson and O'Keefe, 2009). We hypothesize that the MS approach may average out the site-based variability, and thus provide one consistent PFT-generic parameter vector that can be used for global simulations (e.g. Kuppel et al., 2014).

4

2 Methods and Data

2.1 ORCHIDEE Terrestrial Biosphere Model

ORCHIDEE is a global process-oriented TBM (Krinner et al., 2005) and is the land surface component of the IPSL-CM5 Earth System Model (Dufresne et al., 2013). In this study we used the "AR5" version that was used for the IPCC Fifth Assessment Report (Ciais et al., 2013). The model calculates carbon, water and energy fluxes between the land surface and the atmosphere at a half-hourly time step. The water and energy module computes the major biophysical variables (albedo, roughness height, soil humidity) and solves the energy and hydrological budgets. The carbon module controls the uptake of carbon into the system and respiration following cycling of C through the litter and soil pools. Carbon is assimilated via photosynthesis depending on light availability, CO_2 concentration and soil moisture, based on the work of Farquhar et al. (1980) for C3 plants and Collatz et al. (1992) for C4 plants. The module includes the calculation on a daily time step of a prognostic LAI and allocation of newly-formed photosynthates towards leaves, roots, sapwood, reproductive structures and carbohydrate reserves, depending on the availability of moisture, light availability and heat (Friedlingstein et al., 1999). The phenology models that control the timing of leaf onset and senescence in ORCHIDEE, depending on PFT, were described in Botta et al. (2000) and Maignan et al. (2011) but are described in more detail in Appendix A. The simulated fAPAR can be calculated from the model LAI using the following Beer-Lambert extinction law, assuming a spherical leaf angle distribution and that the sun is at nadir (following Bacour et al., 2015):

$$fAPAR = 1 - e^{-0.5.LAI} \qquad (1)$$

ORCHIDEE's functioning relies on the concept of Plant Functional Types (see Wullschleger et al. (2014) for a review). A PFT groups plants that have the same physiological behaviour under similar climatic conditions. ORCHIDEE uses 13 PFTs that are listed in Table 1 (along with the phenology model used). Different PFTs share the same processes but usually with different parameter values, except for the phenological models that are PFT-dependent (Table 1). The model is driven by meteorological variables related to temperature, precipitation, short- and long-wave incident radiation, specific humidity, surface pressure and wind speed. Soil texture and PFT fraction are also prescribed per grid cell.

Natasha MacBean 5/11/2015 16:49
Deleted: , in revision

2.2 Satellite data

2.2.1 Observing the seasonal cycle of vegetation

The seasonal cycle of the terrestrial vegetation is observed daily, cloud cover permitting, at a global scale and medium-scale spatial resolution (250m) from several polar orbiting spectroradiometers. Studies have shown that considerable discrepancies exist between so-called "high-level" satellite products such as LAI or fAPAR, especially when considering their magnitude (D'Odorico et al., 2014; Garrigues et al., 2008; Pickett-Heaps et al., 2014). This is because radiative transfer models are used to derive these products, which introduces uncertainty due to undetermined parameters or potentially incomplete descriptions of the radiative transfer model physics. Instead therefore, we considered a vegetation greenness index, the Normalized Difference Vegetation Index (NDVI), that is directly related to the near infrared (NIR) and red (RED) surface reflectance, ρ ($NDVI = \rho NIR - \rho RED / \rho NIR + \rho RED$). This index is based on the fact that photosynthesising vegetation reflects a high proportion of the incoming NIR radiation, whilst absorbing most of the red. NDVI has been shown to be linearly related to fAPAR, though with uncertainties related to the issues mentioned above (Fensholt et al., 2004; Knyazikhin et al., 1998; Myneni and Williams, 1994). Therefore although NDVI is not directly related to a physical property of the vegetation, it does capture its seasonal cycle together with inter-annual anomalies, and therefore can be used to optimise the model phenology (via the simulated fAPAR). In order to optimise the seasonality (but not the magnitude) of modelled daily fAPAR using the NDVI data, we normalize both to their maximum and minimum values of the whole time series at each site (following Bacour et al., 2015).

2.2.2 MODIS NDVI data and processing

NDVI observations are derived from the MOD09CMG collection 5 (v5) surface red (620-670nm) and Near-Infrared (841-876 nm) daily global reflectance products available at 5km from the MODerate resolution Imaging Spectrometer (MODIS) on-board the NASA's Terra satellite. The reflectance data were cloud-screened and corrected for atmospheric and directional effects (related to the change of reflectance with observation geometry) following (Vermote et al., 2009), and the corresponding NDVI was calculated for the 2000-2008 period. The time series were interpolated on a daily-basis, in order to account for any missing values

6

Natasha MacBean 9/11/2015 11:34
Deleted: and

Natasha MacBean 9/11/2015 11:37
Deleted: vegetation parameter

Natasha MacBean 9/11/2015 11:38
Deleted: but

Natasha MacBean 5/11/2015 11:44
Deleted: compare

Natasha MacBean 5/11/2015 11:44
Deleted: to

Natasha MacBean 5/11/2015 11:47
Deleted: , in revision

Natasha MacBean 4/11/2015 17:23
Deleted: s

Natasha MacBean 4/11/2015 17:23
Deleted: BRDF

due to cloud, using a third degree polynomial and considering the ten nearest valid acquisitions, with a maximum allowed difference of fifteen days. The NDVI values were then spatially averaged at the model forcing spatial resolution (0.72°) for each timestep. The data has a noise range of ~0.025 to 0.03, with highest values in densely forested areas (Vermote et al., 2009). However, in this study the daily model and observation uncertainty used in the assimilation was defined as the RMSE between the normalized prior model fAPAR simulation (using default ORCHIDEE values) and the normalized NDVI observations, following (Kuppel et al., 2012). This error thus accounts for the spatial and temporal averaging, the error of the NDVI retrieval and the model structural error.

2.3 Data assimilation procedure

2.3.1 System description

The ORCHIDEE Data Assimilation System (http://orchidas.lsce.ipsl.fr) is based on a variational data assimilation procedure that has been described in detail in previous studies using ground-based net surface CO_2 and energy fluxes (Kuppel et al., 2012; Santaren et al., 2007; Verbeeck et al., 2011). Kuppel et al. (2012) presented the first results using a multi-site (MS) version of the system at selected eddy-covariance flux tower locations, where data from all sites were used to optimize the model parameters at the same time for each PFT. As with most statistical data assimilation approaches it follows a Bayesian framework, where prior knowledge of the parameter values is updated based on new information from the observations. Assuming that the probability distribution functions (PDFs) of the model parameter and observation uncertainties are Gaussian, the optimal parameter vector x can be found by minimizing the following cost-function $J(x)$ (Tarantola, 1987):

$$J(x) = \frac{1}{2}[(H(x) - y).\mathbf{R}^{-1}.(H(x) - y)^T + (x - x_b).\mathbf{P}_b^{-1}(x - x_b)^T] \quad (2)$$

where y is the observation vector, $H(x)$ the model outputs, given parameter vector x, $\mathbf{R}$ the uncertainty matrix of the observations (including observation and model errors), x_b the *a priori* parameter values (the standard values of ORCHIDEE) and $\mathbf{P_b}$ the *a priori* uncertainty matrix of the parameters. Hence, the cost function describes the misfit between the observations and corresponding model outputs, plus the misfit between the current and prior

7

parameter vectors, weighted by prior information on the parameter and observation uncertainties. Observation and model errors are assumed to be uncorrelated in space and time, and parameters are assumed to be independent; hence $\mathbf{R}$ and $\mathbf{P_b}$ are diagonal matrices. The cost function is iteratively minimized using the gradient-based L-BFGS-B algorithm (Byrd et al., 1995), which allows the definition of boundary constraints for the parameters. The prior parameter vector is most commonly used as the starting point in the iterative minimisation, but it can be started from any point (set of parameter values) in the parameter space. The gradient of the $J(x)$ is estimated using the Tangent Linear model, except for parameters that impose a threshold on the model processes. For these, the finite difference method is used.

The posterior parameter covariance can be approximated from the inverse of the second derivative (Hessian) of the cost function around its minimum, which is calculated using the Jacobian of the TBM model with respect to fAPAR at the minimum of $J(x)$ (for the set of optimized parameters), $\mathbf{H}_{\infty}$, following Tarantola (1987):

$$\mathbf{P}_{post} = [\mathbf{H}_{\infty}^{T}\mathbf{R}^{-1}\mathbf{H}_{\infty} + \mathbf{P}_{b}^{-1}]^{-1} \tag{3}$$

The posterior parameter covariance can then be propagated into the model state variables (fAPAR or net C flux) space given the following matrix product and the hypothesis of local linearity (Tarantola, 1987):

$$\mathbf{R}_{post} = \mathbf{H}.\mathbf{P}_{post}.\mathbf{H}^{T} \tag{4}$$

The square root of the diagonal elements of $\mathbf{R}_{post}$ corresponds to the posterior error (standard deviation σ), on the state variables considered of each grid cell. In order to appraise the knowledge improvement brought by the assimilation, the error reduction is determined as 1 – $\mathbf{R}_{post}$ / $\mathbf{R}_{prior}$).

2.3.2 Parameters to be optimized

Figure 1 shows a general schematic of how the parameters of the phenological equations used in ORCHIDEE (Botta et al., 2000) control the timing of the seasonal cycle of the LAI as well as the rate of leaf growth and fall. The parameters that are optimized for each PFT are given in Table 2 and are briefly described here. A more detailed description can be found in Appendix A. The start of the seasonal cycle of temperature-driven PFTs is constrained by

8

1   optimizing the Growing Degree Day threshold, $GDD_{threshold}$ (equations A1 and A2), the

2   threshold for the Number of Growing Days, $NGD_{threshold}$ and the $LAI_{threshold}$ (equation A4)

3   parameters, which all play a part in controlling leaf onset and rate of canopy growth. As the

4   $GDD_{threshold}$ is calculated in different ways depending on the PFT-dependent phenology model

5   used, and as the $NGD_{threshold}$ acts in a similar way to the GDD models, we introduced one

6   single multiplicative effective parameter, K_{pheno_crit}, to optimize the $GDD_{threshold}$ and

7   $NGD_{threshold}$ for *all* phenology models. Thus the $GDD_{threshold}$ and the $NGD_{threshold}$ become:

8
$$GDD_{threshold} = K_{pheno\_crit}.GDD_{threshold} \qquad (5)$$

9
$$NGD_{threshold} = K_{pheno\_crit}.NGD_{threshold} \qquad (6)$$

10   with an *a priori* value of 1. In a similar manner a new effective parameter, K_{lai_happy} was

11   introduced to compute the $LAI_{threshold}$ parameter, which is the LAI below which the

12   carbohydrate reserves are used for leaf growth at the beginning of the growing season,

13   following the equation:

14
$$LAI_{threshold} = K_{lai\_happy}.LAI_{max} \qquad (7)$$

15   Although it's not strictly a phenology model parameter, we optimise K_{lai_happy} as it is partly

16   responsible for the rate of leaf growth. LAI_{max} is a fixed parameter in this study as we only

17   examine the seasonal cycle of the vegetation, not its magnitude.

18   The end of the seasonal cycle is constrained by optimizing the critical leaf age for senescence,

19   $L_{agecrit}$ (equation A5), the senescence temperature threshold, $T_{threshold}$ (equation A6) and the

20   rate of leaf fall, L_{fall} (equation A8) parameters. $L_{agecrit}$ and L_{fall} are optimized directly, and

21   $T_{threshold}$ is optimized through the C_0 parameter (equation A6), and is henceforth called T_{senes}.

22   For phenology models that are driven by soil moisture conditions ("MOI" models – see

23   Appendix A and Table 1) the parameter that controls leaf onset is the "minimum time since

24   the last moisture minimum" ($Moist_{Tmin}$), and the parameters that control senescence are

25   $Moist_{senes}$ and $Moist_{no\_senes}$, the critical moisture levels below and above which senescence

26   does and does not occur, respectively. These PFT-dependent parameters are optimized

27   directly, i.e. no effective parameters are introduced to scale the original ORCHIDEE

28   parameter.

29   The prior parameter values are taken from the ORCHIDEE standard (non-optimized) version

30   and are detailed in Table 2. The maximum and minimum bounds of the parameters were set

9

1 based on literature and "expert" knowledge. Prior uncertainty on the parameters was taken to

2 be 40% of the parameter range following Kuppel et al. (2012).

3

2.3.3 PFTs optimized and site selection

5 The six deciduous, non-agricultural PFTs of ORCHIDEE are optimized in this study. For

6 each of the PFTs that were optimized we selected thirty sites (where one site is equal to one

7 model grid cell at 0.72^{o} resolution – see Section 2.4) that fulfilled several constraints (Figure

8 2). First the grid cells have to be representative of the considered PFT and thus contain a high

9 fraction of the PFT in question. This was mostly >0.6 except for the Boreal Broadleaved

10 Deciduous (BoBD) PFT where the fractional cover is never greater than 0.4. For this PFT, all

11 the grid points selected contained 40% BoBD trees and high fractions (0.5-0.6) of natural C3

12 grasses (NC3), thus both PFTs were optimized for these grid cells simultaneously. Second,

13 the site locations should be as representative as possible of the PFT spatial distribution. This

14 is achieved by a random sampling of grid cells with a fractional coverage above the given

15 threshold. Lastly each NDVI time series was visually inspected and discarded if it was too

16 noisy or contained an incomplete seasonal cycle. Whilst we could not be 100% certain that no

17 land cover change or disturbance had taken place for the grid cells selected, none of the time

18 series showed discernible signs of a shift in vegetation. Fifteen of the sites were used in the

19 optimisation, and the other fifteen were kept for spatial validation following the optimisations

20 (see Figure 2). To separate the thirty sites into two sets of fifteen for optimisation and

21 validation, we ordered all sites by their grid cell row number and took alternate points for

22 each list.

23

2.4 Optimisations and simulations performed

25 In this study ORCHIDEE is used in forced offline mode and is driven by 3-hourly ERA-

26 Interim meteorological fields (Dee et al., 2011), on a regular 0.72° grid, which are linearly

27 interpolated to a half hour timestep within ORCHIDEE. We use the Olson land cover

28 classification, which contains 96 classes at a resolution of 5 km, to derive the PFT fractions at

29 0.72^{o} following (Vérant et al., 2004). The soil texture classes are derived from Zobler (1986).

10

1   The impact of land use change, forest management, harvesting and fires were not included in
2   any simulation.

2.4.1 Multi-site optimisation

4   For each PFT optimized, the fifteen optimisation sites (see Section 2.3.3) were first optimized
5   simultaneously (i.e. all sites were included in the same cost function), over the 2000 – 2008
6   period using the multi-site (MS) approach detailed in Kuppel et al. (2012). Following
7   (Santaren et al., 2014) we tested the ability of the algorithm to find the global minimum of the
8   cost function by starting the iterative minimisation algorithm (see Section 2.3.1) at different
9   points in the parameter space, choosing twenty random "first guess" sets of parameters and
10 performing a MS optimisation for each. The results of these tests are presented in Section 3.1.

11

2.4.2 Single-site optimisation

13 A single site (SS) optimisation was then performed for each of the same fifteen optimisation
14 sites. The assimilations were exactly the same as for the MS optimisation, except each site
15 was optimized separately. The posterior parameter vector resulting from the "best" random
16 first guess MS optimisation (taken as the greatest % reduction in the cost function) was used
17 as the first guess for the SS optimisation. The first guess with the greatest % reduction in the
18 cost function was equivalent to the first guess that resulted in the lowest value of the cost
19 function, as the % reduction was calculated using the value of the cost function using the
20 default (prior) ORCHIDEE parameters.

21

2.4.3 Site-based validation

23 The same MS posterior parameter vector for each PFT was then used to perform a simulation
24 at each of the fifteen extra spatial validation sites (see Section 2.3.3) over the same time
25 period. In addition, prior and posterior simulations at all thirty optimisation and validation
26 sites were extended to cover the 2009 – 2010 period in order to perform a temporal validation.

27

Natasha MacBean 5/11/2015 11:54
Deleted: vectors

11

2.4.4 Global-scale evaluation

Finally two global-scale simulations (with increasing atmospheric CO_2 concentration and changing climate) were performed for the 1990 – 2010 period with both the prior and MS posterior parameter values, in order to evaluate the impact of the optimisation on the global mean patterns and trends in annual mean fAPAR, amplitude and GSL. The same ERA-Interim 0.72^o forcing data were used as for the site-based optimisations. Note that no spinup of the soil C pools was needed for this study.

2.5 Post-processing and analysis

The prior and posterior RMSE and correlation coefficient, R, were calculated for both the MS and SS optimisations at all sites for a comparison. The values for the spatial and temporal validation simulations were evaluated to assess the spatial and temporal generality of the posterior vectors. For all the analyses performed in this study, metrics given per PFT at global scale were derived for grid cells that contained >= a certain PFT fraction following the rules used to select the optimisation sites (see Section 2.3.3).

2.5.1 Calculation of the start of leaf onset and senescence, GSL and trend analysis

The curve-fitting method of (Thoning et al., 1989) was used to fit a function to the daily time series of observations and model output as described in (Maignan et al., 2008). The function consists of two parts; a second-order polynomial that is used to account for the long-term trend, and a fourth order Fourier function to approximate the annual cycle. The residuals of the fit to this function were filtered with two low pass filters in Fourier space (80 and 667 cut-off days) and then added back to the function to produce a smoothed function that captures the seasonal and inter-annual variability and long-term trend. The detrended curve can be calculated by subtracting the trend from the smoothed function. The Start of Season (SOS – leaf onset) and End of Season (EOS – the start of leaf senescence) were defined as the upward and downward crossing points of the "zero-line" of the de-trended curve per calendar year (see Figure 1 in Maignan et al., 2008). These values were calculated for all grid cells with only one seasonal cycle per year (this includes grid cells in the SH where the growing season

spans two calendar years). The GSL was calculated as the number of days per calendar year when the detrended curve is greater than zero. Therefore unlike the SOS and EOS, the GSL was also calculated for grid cells that contain multiple growing seasons within a calendar year.

For the trend analysis, a linear least squares regression was used to calculate the long-term trend in the annual fAPAR amplitude, Growing Season Length (GSL) and the mean fAPAR time series.

2.5.2 Global evaluation with MODIS NDVI

The global simulations were evaluated with the same MODIS NDVI data as were used at site-level for the optimisation, following the protocol of (Maignan et al., 2011). The following metrics were used for evaluation of both the prior and posterior simulations:

- The correlation between the normalized simulated fAPAR and MODIS NDVI weekly time series.
- The bias (in days) between the modelled and observed SOS and EOS dates (model – observations) were also examined so as to investigate the impact on the timing of the phenology more directly (a positive bias indicates the model date is later than the date calculated from the observations).

The above metrics were calculated for each grid cell. Following this a global median value was calculated, as well as a median correlation per PFT.

3 Results

3.1 Convergence of the optimisation algorithm

We initially tested the ability of the MS optimisation to find the global minimum of the cost function ($J(x)$) by starting at 20 different random "first guess" points in the parameter space. For the forest PFTs and natural C3 grasses the final cost function value was mostly within ~30% of the minimum (lowest) cost function value (up to 50% for TeBD – Table 3, 2nd

13

column), and in the majority of cases a 30-60% reduction in the cost function was achieved (Table 3, 3rd column). The skill of the optimisation algorithm is highly dependent on the PFT in question; the lowest final value of the cost function and the highest % reduction (normalized to the value of *J(x)* for the default parameters of ORCHIDEE) across all 20 random tests was seen for the BoND PFT. There was a higher spread in the % reduction for natural C3 grasses and the TeBD PFTs, suggesting the cost function is not as smooth (i.e. contains more local minima) as for the BoND PFT (for example). This is possibly linked to the need for a greater number of species for certain PFTs or due to differing parameter sensitivities under different climate regimes (the NC3 sites have a particularly wide global distribution). Nevertheless, examining these results we feel confident that for these PFTs the assimilation system converges to a value of the cost function that is reasonably close to the likely global minimum. Thus for the SS optimisations, the site-based validation and the global-scale evaluation we used the MS posterior vector that resulted in the minimum value of the cost function.

However the picture is different for natural C4 grasses (NC4). Only 2 out of the 20 random first guess tests resulted in a >10% reduction in the cost function, and although the spread of final values of the cost function was low and close to the minimum value (Table 3, column 2), the final value was between 2 and 10 times higher than that achieved for other PFTs (Table 3, column 1). This suggests that the optimisation algorithm cannot find a better fit to the data than with the default parameter values. It is possible that the BFGS algorithm is not adequate for exploring the parameter space for NC4 grasses, but given that none of the random tests resulted in a noticeable reduction in the cost function, it is more likely that the model sensitivity to the parameters is lower than for other PFTs. This in turn suggests that the phenology model structure itself is inadequate for this NC4 grasses.

3.2   Improvement in the model-data fit at site level

3.2.1 Temperate and boreal PFTs

There is an improvement in the model-data fit after both SS and MS optimisations for all temperate and boreal broadleaved and needleleaved deciduous forests (TeBD, BoND, BoBD) and for natural C3 grasses (NC3), largely resulting from an earlier onset of senescence in the model and therefore a substantially shortened growing season length (Figure 3 and Figure 4).

14

1　The shift in the start of leaf growth is much smaller, which is not surprising as the prior model

2　more closely matches the observations. Of the four PFTs listed above, only TeBD trees have a

3　slightly later leaf onset as a result of the optimisation. Figure 3 shows the full time-series at

4　one site of both the normalized and un-normalized fAPAR and NDVI, together with the

5　simulated LAI, for the BoBD PFT. This site is provided as an example of the typical changes

6　in temporal behaviour seen for the four PFTs listed above. Figure 4 shows the mean seasonal

7　cycle of the normalized fAPAR/NDVI across all sites and years (2000 – 2008) for each of the

8　four PFTs and demonstrates that the patterns seen in Figure 3 are similar for all the boreal and

9　temperate deciduous PFTs.

10　The optimisations resulted in a significant reduction in the RMSE (34-61%) and increase in

11　correlation (posterior R > 0.82) between the normalized modelled fAPAR and MODIS NDVI

12　data for all four temperate and boreal PFTs (Table 4). The variation in the RMSE and R at

13　each site for prior, multi-site optimisation and the spread for all the single-site optimisations

14　for all four PFTs are shown in Figure S1. The improvement is greatest for the Boreal PFTs

15　(median reduction in RMSE across all sites for both SS and MS optimisations of ~50-60%

16　and an increase in R from 0.41 to 0.9), but nonetheless the optimisations of the temperate

17　broadleaved deciduous (TeBD) and natural C3 grasses (NC3) PFTs result in a median

18　reduction of uncertainty of between ~20-40% and an increase in R of up to ~0.2.

19　There is a discernible slowing down in the rate of leaf growth towards the end of the leaf

20　onset after the assimilation, which particularly results in an improved fit to the observations

21　for the TeBD, BoND and NC3 PFTs. However it is noticeable that although parameters that

22　partially control the rate of leaf growth and fall are included in the optimisation, the model

23　generally grows and sheds leaves too fast compared to the observations, except for the BoBD

24　PFT, which results in the model having an unnatural "box-like" temporal profile (Figure 4

25　and see Section 4.3 for further discussion).

26　The MS optimisation (red line in Figure 3 and Figure 4) largely results in a similar reduction

27　in RMSE and increase in R as the SS optimisations at each individual site except for TeBD

28　trees, although a similar magnitude of improvement is achieved for this PFT as for the others

29　(Table 4 and Figure S1). This suggests that the MS parameter vector is universal enough to be

30　used to perform global simulations.

31

15

3.2.2 Tropical deciduous forest and C4 grasses

For both the tropical broadleaved raingreen (TrBR) and natural C4 grass (NC4) PFTs, the median prior fAPAR simulation performs reasonably well compared to the observations, with RMSEs of 0.29 and 0.23 and R of 0.73 and 0.81 respectively (Table 4 and Figure S1). Following optimisation there is an improvement in the median model-data misfit both for the SS and MS optimisation for TrBR trees across all sites, but the spread in posterior RMSE and R-values remains high (Figure S1). Figure 5a shows an example of the typical issues seen for some TrBR sites that have not been resolved by optimizing the phenological parameters. The growing season is always slightly out of phase, even after the optimisation, with the simulated SOS and EOS lagging that of the observations. The observed start of leaf growth coincides with the start of increased precipitation, as would be expected, but the simulated onset does not, despite the fact that the onset phenology model is solely driven by soil water availability. Possible causes of inconsistencies in the model will be discussed in Section 4.4. At the end of the growing season the optimisation results in a more gradual start of leaf turnover at many sites, thus better matching the observation temporal profile, but still the end of the leaf fall lags that of the observations (Figure 5a). Finally at some of the sites the observations show a smaller, second period of growth in some years (not shown), but the model also does not capture this.

There is no change in the median RMSE and R for the NC4 PFT with the MS optimisation, although the prior model-data misfit is relatively small (Figure S1). The SS optimisations do result in a small reduction in the median RMSE (0.21) but no improvement in the median correlation. This is not surprising given the results of the random first guess tests presented in Section 3.1. A comparison of the observed and modelled time-series of NDVI and fAPAR at each site again reveals where the model is not able to fully reproduce the seasonality seen in the observations. At many sites the model predicts a positively biased (i.e. too late) SOS, followed by a drop in fAPAR in the first half to middle of the year that is not seen in the observations, and does not correspond to a decline in precipitation (e.g. Figure 5b). The optimisation can result in the partial removal of this feature, particularly for SS optimisations at certain sites, but at the expense of a further delay to the start of leaf growth. Neither the SS or MS optimisations are able to reduce the model-data misfit by forcing an earlier start of senescence at any of the sites. As there is no discernible improvement after the MS optimisation of the NC4 PFT, the posterior parameters are not used in the further analysis of

16

1 global changes to the GPP, GSL or trends. It is likely that the phenology models that are used

2 in water limited ecosystems (TrBR and NC4) need revising (see discussion in Section 4.4).

3

3.3 Validation of the optimised phenology

3.3.1 Spatial and temporal validation

6 Table 4 also shows the RMSE and R for the extra 15 sites that were not included in the

7 optimisation (spatial validation), and for all sites for the period 2009 – 2010 that were not

8 included in the optimisation (temporal validation). These validation exercises were performed

9 with just the MS posterior parameter vector for each PFT. Similar magnitudes and patterns of

10 improvement are observed between the PFTs as for the sites used for optimisation – the

11 largest improvement is seen for the BoND PFT, and there is no improvement for NC4

12 grasses. These results again give confidence in the generality of the MS posterior vector and

13 its use in regional and global scale simulations, except for the NC4 PFTs for which there was

14 an insufficient improvement post-optimisation.

15

3.3.2 Validation at global scale with MODIS NDVI

17 The global median correlation between the model and the MODIS NDVI data has increased

18 from 0.56 to 0.67 after the optimisation, demonstrating an overall improvement in the

19 simulated fAPAR time series. As seen at site level, the largest increase in correlation between

20 the modelled and observed time series is for the boreal PFTs. There is also a modest

21 improvement for natural C3 grasses (Table 5). Figure 6 shows the spatial distribution of the

22 correlation for the both posterior simulation and the difference after optimisation (posterior –

23 prior). The difference map shows that R has mainly improved for boreal regions in the north

24 of Canada and in Siberia, the C3 grasslands in central Asia and western North America, and

25 the high altitude regions of the Andes (due to improvements in BoBD, BoND and NC3 PFTs)

26 with slight changes for tropical raingreen trees in savannah-dominated regions in Africa. A

27 decrease in R was seen in part of the drylands of western North America and along the

28 western boundary of South America.

17

The global median End of Season (EOS) bias (model – observations) between the model and MODIS data was reduced dramatically as a result of the optimisation (prior: 33 days; posterior 5 days). Note that a positive bias indicates the model date is later than the date derived from the MODIS data. Again, boreal PFTs and NC3 grasses showed considerable improvement, as expected from the site-level behaviour (Section 3.2), but grid cells containing high fractions of temperate and boreal evergreen trees were also positively affected (Table 6). The bias in the Start of Season (SOS) dates also decreased (prior and posterior global median bias of 22 and 14 days, respectively), with improvements seen for all PFTs except TeBD trees and crops (Table 6).

3.4 Posterior parameters and processes constrained

The prior value, prior range and posterior value from the MS optimisation for each parameter (per PFT) are shown in Table 2. Figure 7 shows the prior and posterior parameter values for both the SS and MS optimisation for each parameter and each PFT. In Figure 7 the mean and standard error of the mean of the SS posterior parameters are shown (circle with error bars), together which the value obtained at each individual site (crosses). For the prior simulation and MS optimisation the error bar corresponds to the standard deviation of the parameter value (calculated using equation 3). The MS uncertainty is lower than spread of SS posterior values, suggesting that it underestimates the true uncertainty of the posterior parameters. This may be the case given the assumptions of linearity of the model and of Gaussian and uncorrelated errors.

The lower posterior values of K_{pheno_crit} reduced the positive bias in the SOS dates, for temperate and boreal deciduous trees and natural C3 grasses, thus providing a better fit to the model. For all temperate and boreal PFTs the posterior value of the K_{lai_happy} parameter, which is used to calculate the LAI value below which leaf growth is supported by the carbohydrate reserves, decreases for both the SS and MS optimisation. In ORCHIDEE the rate of leaf growth slows down after this LAI threshold is reached as the C now comes from photosynthesis, which may be limited by various factors. Lower values of K_{lai_happy} therefore result in an earlier end to the period of rapid canopy growth at the beginning of the season and thus a smoother temporal profile follows during the final stages of growth. This partially compensates for the "box-like" model behaviour, but structural deficiencies related to spatial

18

variability need to be addressed further (see Section 4.3). The lower value of K_{lai_happy} (together with the earlier start to senescence) is also responsible for the reduction in the peak LAI at some sites for some PFTs, particularly BoND trees (see Figure 3 for example). It may be hypothesised that the optimisation resulted in a reduction in the C allocated to the carbohydrate reserve, which therefore may also have contributed to the decrease in the peak LAI. However an examination of the simulated carbohydrate reserve showed this not to be the case (results not shown). In any case this observed reduction in peak LAI was not a common result of the optimisation when considering all PFTs.

The earlier start of senescence is overwhelmingly caused by an increase of T_{senes} for all temperate and boreal trees and natural C3 grasses in both the SS and MS optimisations, as well as a lowering of the critical leaf age ($L_{agecrit}$), though this is not the case for BoBD trees (Figure 7). It is important to remember however that the optimisations at BoBD sites also included high fractions of natural C3 grass that were optimized at the same time (see methods Section 2.3.3) and therefore the same parameter can have strong interactions between the two PFTs, as can be seen in for the $L_{agecrit}$ parameter in the correlation matrices in Figure S2. The L_{fall} parameter has not changed considerably after the optimisation, suggesting that the rate of leaf fall matches that of the observations when parameters that govern the start of leaf senescence have been optimized. The exception is that of TeBD trees, where the rate of leaf fall has decreased following optimisation (Figure 4a) and thus the model better matches the observations.

The phenology of C3 grasses is also controlled by soil moisture availability. The moisture-related leaf onset parameter, $Moist_{Tmin}$, does not appear to be as important as the temperature-related leaf onset parameter (K_{pheno_crit}). However, the increase in the value of both T_{senes} and $Moist_{senes}$ post-optimisation show that both moisture and temperature conditions are responsible for the marked shortening of the growing season length for natural C3 grasses (Figure 4), as would be expected given the wide geographical distribution of this PFT.

For the tropical raingreen forests (TrBR), there is a decrease in the posterior SS and MS values of $Moist_{Tmin}$ and an increase for the $Moist_{senes}$ parameter, which results in an earlier start of both leaf growth and senescence, again reducing the positive bias in the SOS and EOS dates predicted by the model. However the parameters are "edge-hitting", which suggests the optimisation has not necessarily found the optimum solution. This may explain why the model remains out of phase with the observations as described above (Figure 5a).

19

Although the phenology of C4 grasses is governed by both temperature and moisture conditions, the fact that there is no change in the value and uncertainty of the temperature-related parameters, K_{pheno_crit} and T_{senes} shows a lack of sensitivity to both (Figure 7), which is not surprising as the location of the C4 grasses pixels used in this study are mainly located in moisture-limited tropical regions. The SS and MS posterior values of the moisture-related parameters, $Moist_{Tmin}$ and $Moist_{senes}$, have changed (increased), but the spread of the SS optimized parameter values is large, which accounts for the lack of improvement in the median RMSE and correlation between the time series of the model and observations (Table 4).

3.5 Change in global patterns and trends of mean annual fAPAR, amplitude and GSL

Figure 8 shows the change (posterior – prior) in the mean annual GSL, fAPAR amplitude and mean simulated fAPAR globally over the 1990-2010 period. As expected from the site-level results for temperate and boreal PFTs (Figure 4 and Table 4), there was a strong decrease in the mean GSL in the high latitudes and grasslands across much of the NH (median of -30 and -10 days for boreal (60-90°N) and temperate (30-60°N) regions respectively), as well as in equatorial Africa (median of -28 days) (Figure 8a). An increase in the GSL of ~7 days was mostly observed in the Sahel and Miombo savannah regions of Africa. A decrease in fAPAR amplitude was also seen in Siberia and in water-limited grasslands in southern Africa, the western United States and central Asia (Figure 8b). Although the primary aim of the assimilation was to constrain the timing of the phenology, changes in the amplitude are the result of the interplay between parameters controlling the rate of leaf growth and fall and the timing of senescence that ultimately result in a lower maximum LAI, as discussed in Section 3.4. The combined result was a strong decrease in the annual mean fAPAR in most regions of the globe that are not dominated by evergreen trees, crops or bare soil, except for the Sahelian region in Africa (Figure 8c).

Figure 9 shows the linear trend (yr^{-1}) in the annual mean fAPAR for the 1990 – 2010 period, both for the prior and posterior simulation and their difference. The trends of the annual mean are shown as it is a more comprehensive metric compared to the daily/monthly time-series of fAPAR, the GSL or fAPAR annual amplitude. The large-scale spatial patterns of positive and

negative trends over the 1990 – 2010 period were not altered significantly after the assimilation, however the strength of the trend is generally reduced. This can be seen in Figure 9 as positive "greening" trends mostly correspond to regions where there was a decrease in the slope of the trend after optimisation (orange areas in Figure 9c), and vice versa for negative "browning" trends (purple areas in Figure 9c). This was not always the case however, for example the "greening" trend in central Siberia (around 60°N) and the "browning" trend in parts of the Sahelian both increase in strength following the assimilation. Note that an examination of the trends in other metrics (SOS, EOS, GSL or annual amplitude) did reveal different changes in the spatial patterns following the assimilation. For example the increase in GSL actually increased slightly in north-western Siberia, and the decline in GSL in Mongolia (also seen as a browning trend in the annual mean in Figure 9) increased by ~2-3 days after the optimisation (results not shown). Further details are not discussed here.

We chose not to compare the simulated trends with that of the MODIS NDVI. This was partly because the 2000 – 2010 period is likely too short to calculate a robust trend, as the influence of inter-annual variability will be stronger; indeed the trends over the longer 1990 – 2010 period are more geographically distinct. Secondly it was not the aim of this study to validate the modelled trends, nor would it be appropriate, because we have used a version of the model that does not include land use change, disturbance and other effects that will contribute to changes in vegetation greenness at global scale. The results presented here serve to highlight that different parameter values can change the strength, sign and location of the trends. However, it is worth noting that the sign of the simulated trend does not always match the MODIS data, especially for drier, warmer semi-arid regions. For example, the browning trend seen in the Kazakh Steppe in the MODIS data is stronger in ORCHIDEE and extends further east into Mongolia (results not shown). Similarly, the model predicts a decline in fAPAR across much of sub-Sahelian Africa that is not seen in the MODIS NDVI. The optimisation did not result in a change in the trend direction for this region, though generally it did reduce its strength. Overall the greening trend in the NH (>~30°N) was well captured by the model both before and after optimisation.

21

4   Discussion

4.1   Optimisation performance

Whilst the SS optimisations result in a reduction in the model-data misfit across a range of sites, this study has shown that a MS optimisation can achieve a similar improvement with one unique parameter vector. This is an important result, and reinforces the conclusions of (Kuppel et al., 2014) that the MS posterior parameters can be used with confidence to perform global simulations. Previous site-level optimisations of phenology models have resulted in a wide range of parameterisations of growing degree day sum, chilling requirements and light availability (Migliavacca et al., 2012; Richardson and O'Keefe, 2009), therefore it is difficult to know which values to use for regional-to-global scale simulations. In most cases the MS optimisation averages out the variability due to specific site characteristics. The validation at site and global scale using daily MODIS NDVI data demonstrates the generality of the MS posterior parameter vectors given the ORCHIDEE model structure. This gives confidence in using these values in regional-to-global scale simulations of the carbon and water fluxes and for future predictions with this model.

Although the optimisation resulted in a dramatic improvement in the seasonal leaf dynamics for temperate and boreal ecosystems, the impact in the inter-annual variability (IAV) as a result of the optimisation for any variable – mean annual fAPAR, mean spring/autumn fAPAR, GSL, SOS, EOS – was minimal (results not shown). This was disappointing as generally there is a low correlation in the IAV between ORCHIDEE and the MODIS data, and IAV in spring phenology has been shown to be a dominant control on C flux anomalies (Keenan et al., 2012).

4.2   Validity of the posterior parameters and optimised phenology models

As data assimilation schemes are expected to result in a reduction in the prior data-model misfit it is useful to assess if the posterior parameter values are indeed realistic, which is conditioned on the prior range as well as the interaction (correlation) between the parameters. However validating these values remains difficult, as there is no database that corresponds directly to phenology model parameters, which may have a different meaning in different models.

22

1 Leaf lifespan (LL) however can more easily be measured and therefore can be found in the

2 literature and in plant trait databases (Kattge et al., 2011; Wright et al., 2004). Although leaf

3 lifespan is not the same as the critical age for senescence parameter ($L_{agecrit}$), the leaf lifespan

4 should be similar if not lower than $L_{agecrit}$, and thus serves as a benchmark to a certain degree.

5 Reich (1998) gave 4 – 6 months for cold-temperate and boreal broad- and needleleaved

6 deciduous trees, similar to the mean values for the same functional types in the TRY database

7 (Kattge et al., 2011). These values encompass the range of optimized values for temperate and

8 boreal broadleaved (TeBD and BoBD) PFTs (160 and 240 days respectively, Table 2). The

9 posterior value of $L_{agecrit}$ for the boreal needleleaved (BoND) PFT was lower than this range

10 at 90 days, and was at the lower boundary of the parameter range. The TRY database gives a

11 mean value of 3.85 and 1.68 months for C3 and C4 grasses, respectively (Kattge et al., 2011).

12 These values are higher than the posterior value of the C3 grasses (60 days) and lower than

13 the posterior value for C4 grasses (166 days). The values of $L_{agecrit}$ for NC3 and BoND PFTs

14 were therefore too low and it is also notable that the values of T_{senes} were also at their upper

15 bounds for these two PFTs.

16 Most of the posterior values for the moisture-related phenology parameters for the Tropical

17 Broadleaved Raingreen and natural C4 grasses (TrBR and NC4) PFTs were also at their upper

18 or lower bounds, even with liberal parameter bounds due to lack of prior knowledge. For

19 example the posterior value of $Moist_{Tmin}$, the number of days since the last moisture minimum

20 before leaf onset, was unrealistically low at 10 days for TrBR trees. In turn the threshold of

21 relative soil moisture needed for senescence ($Moist_{senes}$) was 0.8 and 0.7% for TrBR and NC4

22 PFTs respectively, which is likely too high. Assuming the prior range of the parameters does

23 encompass the likely variability, such "edge-hitting" posterior parameter values can indicate

24 that other processes may be missing. Indeed certain studies (Galvagno et al., 2013; Rosenthal

25 and Camm, 1997) have suggested that photoperiod is also important in determining autumnal

26 senescence in deciduous conifers (e.g. BoND PFT). Possible deficiencies in the models that

27 control tropical deciduous phenology are discussed further in Section 4.4.

28 In order to better evaluate the model parameterisations, we suggest that the phenology

29 observation and modelling community could engage in an elicitation exercise (O'Hagan,

30 (1998, 2012); http://www.tonyohagan.co.uk/shelf/). This would involve gathering knowledge

31 on parameter ranges of typical phenological model parameters from experts in the field, in

32 order to derive probability distributions of the parameter values. However, even if this

23

1 exercise is carried out, measurements made at the species and site level will be difficult to
2 scale across species and to the coarse resolution used in TBMs.

3 The onset models used for temperate and boreal PFTs in ORCHIDEE are mostly simple
4 spring warming models, though some include a chilling requirement (Table 1). Their
5 comparative ability to reproduce the observations could add to evidence that more complex
6 representations including light availability may not be needed (Fu et al., 2012; Picard et al.,
7 2005; Richardson and O'Keefe, 2009). Other studies however have showed improved
8 performance when a photoperiod term was included for species with a late leaf onset (Hunter
9 and Lechowicz, 1992; Migliavacca et al., 2012; Schaber and Badeck, 2003). Several authors
10 (e.g. Fu et al., 2012; Linkosalo et al., 2008) have pointed out that whilst the simple warming
11 onset models may perform well under current climate conditions, future predictions may
12 require additional complexity; for example the model-defined chilling period may not be
13 sufficient in warmer conditions. More importantly perhaps, any model that requires a fixed
14 start date from which thresholds are calculated may be inconsistent under increased
15 temperatures, as warming will start before the defined start date (Blümel and Chmielewski,
16 2012). Ideally therefore these models should also be tested under future warming scenarios,
17 although (Wolkovich et al., 2012) showed the magnitude of species' phenological response to
18 temperature increases is lower in warming experiments compared to historical observations.

19

20 **4.3   Accounting for spatial variability**

21 The coarse-resolution observations used in this study will include the spatial variability in the
22 timing of phenological events for different species within a PFT, or even due to specific site
23 characteristics (edaphic conditions, terrain/slope, local meteorological effects) within the
24 same species (Fisher and Mustard, 2007). During senescence in particular, spatial variability
25 in the rate of leaf fall, and to some extent the leaf colouration, will likely contribute to the
26 decline in "greenness" seen in NDVI observations. ORCHIDEE doesn't explicitly represent
27 this variability, instead vegetation is represented as a mean stand (which is also responsible
28 for the unnatural "box-like" temporal profile seen for some sites/PFTs) and thus the posterior
29 value of L_{fall} parameter likely accounts for such missing structural processes and sub-grid
30 variability. This could explain why the SS optimisations for the TeBD PFT result in a wide
31 variety of values for this parameter (Figure 7). This leads us to question whether phenology

24

should be optimized at the species level (Chuine et al., 2000; Olsson et al., 2013), and/or whether there is a need to include a term that accounts for spatial variability in the model (e.g. Knorr et al., 2010). If the phenology models were optimized at species level there would need to be an increase in the number of points included in the optimisation in order to properly account for the variability between grid cells, which may result in strong correlations between the same parameters shared by the different species (e.g. Figure S2c). On the other hand, prescribing a spatial variability term is a non-trivial issue, as it would not only encompass physiological differences between species but also variation in other site characteristics, as mentioned above. These issues have previously been discussed (e.g. Morisette et al., 2009; Bacour et al., 2015).

4.4   Phenology in ecosystems driven by water availability

The processes that govern leaf phenology in ORCHIDEE cannot reproduce the observations as well in regions where moisture availability, and not temperature, is likely the dominant control. The optimisation has revealed structural deficiencies as the probable cause of inaccurate simulations, rather than incorrect parameter values. In addition to problematic, "edge-hitting" posterior parameter values (see Section 4.2) the prior and posterior model incorrectly simulates a strong decline in vegetation productivity in the Sahelian region, which is opposite to that seen in satellite observations (results not shown, but see (Traore et al., 2014a). Traore et al. (2014a) suggested that incorrect trends predicted by ORCHIDEE could be related to the phenology models, however this study shows that is not the case. Even without a comparison to observations, ORCHIDEE does not always appear to have the correct response to precipitation, with two periods of simulated growth seen in one rainy season but without any decline in rainfall. This unexpected model behaviour is not corrected by the optimisation and needs investigating.

It is likely that the phenology models in ORCHIDEE are too simplistic for these regions and/or that the computation of soil water availability or the plant water stress function are inadequate. Such issues are likely encountered in other TBMs as they rely on similar models. Knorr et al. (2010) pointed out that evaporative demand, and not just moisture availability, should be considered in phenology models. (Traore et al., 2014b) evaluated the inter-annual variability of the soil moisture of ORCHIDEE across Africa using satellite-derived estimates,

25

1 and found that the new 11-layer hydrology version performed better than the 2-layer version
2 that was used in this study. The latest version of ORCHIDEE (Naudts et al., 2015) has a more
3 mechanistic representation of plant water stress using water potential in the soil-plant
4 continuum, which may lead to better predictions of leaf dynamics in drought-prone regions.

5 Although there are fewer studies focusing on the modelling of plant moisture-availability
6 driven phenology, some models do exist for the dry tropics/semi-arid regions. Such models
7 aim to simulate the vegetation response to soil and groundwater availability or atmospheric
8 demand, both empirically (Archibald and Scholes, 2007; Do et al., 2005), or in a more
9 mechanistic way by including non-linear feedbacks via transpiration (Choler et al., 2010).
10 Similar approaches could be included in TBMs in order to better represent leaf growth and
11 turnover in semi-arid grassland and savannah ecosystems in the dry tropics.

12

4.5 Importance of constraining phenology for global change studies

14 Observed increases in GSL and/or increases in vegetation density have been shown to result
15 in concurrent impacts on the C surface fluxes on seasonal time scales (Dragoni et al., 2011;
16 Piao et al., 2007; Richardson et al., 2009), although the magnitude and sign of the effect on
17 net C fluxes is still a topic of debate (see Barichivich et al., 2013; Keenan et al., 2014; Piao et
18 al., 2008; Richardson et al., 2010; White and Nemani, 2003). An in-depth analysis of the
19 impact of the modified leaf phenology on the C, water and energy cycles and the subsequent
20 feedbacks to the atmosphere was beyond the scope of this study. However, the changes in leaf
21 phenology described above resulted in a ~10 PgC yr^{-1} decrease in the simulated global mean
22 annual GPP (uptake of C) over the 1990 – 2010 period (prior: 172.2 PgC yr^{-1}, posterior: 162.5
23 PgC yr^{-1} calculated using PFT fraction- and area-weighted fluxes for each grid cell).
24 Reductions in GPP (results not shown) follow the same global spatial pattern as the difference
25 in annual mean fAPAR (Figure 8c). The decline in GPP is predominantly caused by the
26 shorter GSL in the high latitudes and grasslands across the NH (median of -30 and -10 days
27 for boreal and temperate regions respectively), and in equatorial Africa and western South
28 America (Figure 8a). The exception to this is eastern Siberia where the decrease in fAPAR
29 amplitude, due to the lower peak LAI for BoND trees discussed in Section 3.4, contributes to
30 an even stronger reduction in GPP. In east Africa and South America, the lower fAPAR
31 amplitude is predominantly responsible for the decrease in GPP. The mean annual GPP only

Natasha MacBean 10/11/2015 12:29
Deleted: – results not shown

26

increased in the Sahel and northern Australia, which is due to the fact that the optimisation resulted in an increase in both the GSL and fAPAR amplitude in these regions (Figure 8). The decrease in GPP per day change in the GSL (ΔGPP/ΔGSL) was ~3-4 gCm^{-2}d^{-1} for boreal and temperate regions and an increase of ~2 gCm^{-2}d^{-1} in the Sahel. Large variations in this ratio are seen across the NH depending on the PFT in question, owing to their different physiologies (TeBD: 31 gCm^{-2}d^{-1}; BoBN: 10 gCm^{-2}d^{-1}; BoBD: 5 gCm^{-2}d^{-1}; NC3: 3 gCm^{-2}d^{-1}). The reduction in the mean annual GPP (1990-2010) partially accounts for the large positive bias in ORCHIDEE compared to data-driven global estimates of ~120PgC yr^{-1} (Jung et al., 2011). Note also that the increase in time series correlation and reduction in the bias of SOS and EOS dates have resulted in a improvement in the timing and magnitude of the simulated GPP and ET compared to the data-driven product (Jung et al., 2009). We suggest therefore that the bias in the timing of simulated onset and senescence and GPP estimates in other TBMs, as seen in the Richardson et al. (2012) model intercomparison for example, would be reduced if the phenology-related parameters were optimized using a similar framework. Also, the impact on energy and water fluxes in particular could result in strong feedbacks to climate (Peñuelas et al., 2009), possibly leading to different predictions under future warming.

Aside from making predictions of the carbon, water and energy budgets, TBMs are routinely used in trend attribution studies. A good example in this context would be the exploration of the causes of "greening" or "browning" trends in vegetation productivity (Hickler et al., 2005; Piao et al., 2006), or the impact of such trends on resource use efficiency (Traore et al., 2014b) or the C cycle (Piao et al., 2007). The fact that the optimisation resulted in changes in the strength and location of these trends (Figure 9) demonstrates that such analyses are partly dependent upon model parameters, which can be a considerable source of uncertainty (Enting et al., 2012).

5   Conclusions

This study has demonstrated that a time series of normalized coarse-resolution satellite NDVI data can be used to optimize the parameters of phenology models commonly used in TBMs, and crucially that a multi-site optimisation can find a unique parameter vector that enables better predictions of the seasonal leaf dynamics at global scale. This type of model calibration

framework is thus imperative for earth system model development. The results also highlight that optimizing the parameters allows model developers to distinguish between inaccurate model representations resulting from incorrect parameter values and model structural deficiencies. In ORCHIDEE the models used for predicting the leaf phenology in temperate and boreal regions are able to reproduce the seasonal cycle of the vegetation well after calibration, but ecosystems driven by water availability require further modification, particularly for natural C4 grasses. The optimisation also led to changes in the strength and location of "greening" and "browning" trends in the model, suggesting caution should be exercised when using un-calibrated models for trend attribution studies. Furthermore, the observed trends were not well captured in some regions, which is a key aspect to improve upon when considering future simulations of climate, CO_2 and anthropogenic change.

28

Appendix A: Phenology models in ORCHIDEE

A1. Leaf onset

In temperate and boreal regions the onset of leaves is mainly driven in the spring by an accumulation of warm temperatures (see the review of Hänninen and Kramer (2007)). The well-known Growing Degree Days (GDD) model (Chuine, 2000) sums up the temperatures above a given temperature threshold, T_0 (for example 0°C), starting at a given date (for example the first of January in the Northern Hemisphere). The onset of leaves starts when the GDD reaches a plant/PFT-specific threshold. In ORCHIDEE, T_0 is -5°C, and the GDD sum is calculated from the beginning of the dormancy period, which starts when the leaves were lost or when GPP decreased below a certain threshold.

This simple model may be refined. For example the GDD threshold has been reported to depend on a "chilling requirement" for some species, i.e. their physiology requires cold temperatures to trigger the mechanism that will allow budburst to occur (e.g. Orlandi et al., 2004). This ensures that the dormancy has been broken after a required cold period, and thus prevents a too early awakening. The Number of Chilling Days (NCD) GDD model initiates leaf onset earlier with an increase in the number of chilling days, defined as a day with a daily mean air temperature below a PFT-dependent threshold accumulated after a given starting date (e.g. Botta et al., 2000; Cannell and Smith, 1986; Murray et al., 1989). The GDD threshold therefore decreases as NCD increases. This experimental relationship is a negative exponential with three PFT-specific parameters (Botta et al., 2000):

$$GDD_{threshold} = \frac{A_0}{e^{A_1 NCD}} - A_2 \qquad (A1)$$

where A_0, A_1 and A_2 are parameters that have been calibrated against satellite data (Botta et al., 2000). The growing season begins if the daily calculated GDD is higher than the calculated $GDD_{threshold}$. This model (hereafter referred to as the "NCD_GDD" model) is used for the temperate and boreal broadleaved deciduous (TeBD and BoBD) PFTs in ORCHIDEE.

The start of the growing season for the boreal needleleaved deciduous (BoND) PFT occurs when the number of growing days (NGD), i.e. days with a mean daily temperature above the threshold temperature, T_0 (-5°C), has exceeded a PFT-dependent threshold ($NGD_{threshold}$). The NGD is calculated from the beginning of the dormancy period. This model (hereafter referred

29

1 to as the "NGD" model) was proposed by Botta et al. (2000) for boreal and arctic biomes, and

2 is designed to initiate leaf onset after the end of the soil frost.

3 For C3 and C4 natural grasses and crops (NC3, NC4, AC3, AC4), the GDD threshold is given

4 by a second-degree polynomial of the long term mean annual air surface temperature T_l:

5
$$GDD_{threshold} = B_0 + B_1 T_1 + B_2 T_1^2$$
(A2)

6 where B_0, B_1 and B_2 are PFT-dependent parameters. In addition, leaf onset is initiated only

7 when a moisture availability criterion is met, namely when the moisture minimum occurred a

8 sufficiently long time ago, as specified by a PFT-dependent threshold parameter ($Moist_{Tmin}$):

9
$$\text{time since moisture minimum} \quad > \quad moist_{Tmin}$$
(A3)

10 This moisture availability criterion corresponds to Model 4b in Botta et al. (2000), who

11 assume leaf onset in tropical biomes requires a certain amount of accumulation of water in the

12 soil. Both the moisture availability and GDD threshold criteria (hereafter referred to the

13 "MOI_GDD" model) must be met for leaf onset to occur in grasses and crops.

14 For the tropical broadleaved raingreen (deciduous) (TrBR) PFT, the start of the growing

15 season depends only on the moisture availability criterion (hereafter referred to as the "MOI"

16 model) previously described for grasses and crops.

17 When the onset of leaves is declared, the allocation module first allocates carbon from the

18 carbohydrate reserves towards leaves and roots as long as the LAI is lower than a given

19 threshold, which is a function of the maximum LAI, LAI_{max}, a PFT-dependent value:

20
$$LAI_{threshold} = 0.5 * LAI_{max}$$
(A4)

21 The onset parameter values are listed in Table 2.

22

23 **A2. Leaf age and leaf senescence**

24 To account for the fact that the photosynthetic efficiency of leaves depends on their age, L_{age},

25 they are separated into four age classes. Biomass newly allocated to leaves goes into the first

26 age class and leaf biomass, B_l, is then transferred from one class to the next based on a PFT-

27 specific critical leaf age value, $L_{agecrit}$. The long-term reference temperature modulates the

28 critical leaf age of grasses in order to account for the fact that leaves can live longer in colder

29 climates. The leaf age continually affects the turnover of the leaves both during the growing

30

season and once senescence has begun. Different turnover processes control leaf fall, the first one is a simple aging process based on the $L_{agecrit}$ parameter. For trees, when leaf age is greater than half the critical leaf age a turnover rate is applied following:

$$\Delta B_l = B_l . \min\left(0.99, \frac{\Delta t}{L_{agecrit} \cdot \left(\frac{L_{agecrit}}{L_{age}}\right)^4}\right)$$

(A5)

where ΔB_l is the leaf biomass lost through this aging process and Δt is the daily time step.

The second turnover process is a senescence process (the end of the growing season and the shedding of leaves) that is based on climatic conditions. This only exists for deciduous PFTs. For tree PFTs whose senescence is driven by sensitivity to cold temperatures (TeBD, BoND, BoBD and grasses), senescence begins when the monthly air surface temperature goes below a threshold temperature, defined as a second order polynomial of the long-term mean annual air surface temperature T_l:

$$T_{threshold} = C_0 + C_1 T_l + C_2 T_l^2$$

(A6)

where C_0, C_1 and C_2 are PFT-dependent parameters.

For tropical raingreen trees, the start of leaf senescence is controlled by a lack of availability of water, where the critical moisture availability is calculated as a function of last year's minimum ($Moist_{Tmin}$) and maximum ($Moist_{max}$) moisture availability using the following equation:

$$Moist_{crit} = MIN(MAX(Moist_{min} + 0.5(Moist_{max} - Moist_{min}), Moist_{senes}), Moist_{no\_senes})$$

(A7)

where $Moist_{senes}$ and $Moist_{no\_senes}$ are the PFT-dependent critical moisture levels below and above which senescence does and does not occur, respectively. Once senescence has begun, a fixed turnover rate is applied. Trees lose their fine roots at the same rate as their leaves:

$$\Delta B = B * \frac{\Delta t}{L_{fall}}$$

(A8)

All remaining leaves are shed when leaf biomass becomes too low.

For grasses, the climatic senescence is controlled by both temperature and moisture conditions. The senescence parameter prior values are listed in Table 2. Note that no senescence models in ORCHIDEE currently include a photoperiod term for either onset or senescence.

References

Anyamba, a. and Tucker, C. J.: Analysis of Sahelian vegetation dynamics using NOAA-AVHRR NDVI data from 1981-2003, J. Arid Environ., 63(3), 596–614, doi:10.1016/j.jaridenv.2005.03.007, 2005.

Archibald, S. and Scholes, R. J.: Leaf green-up in a semi-arid African savanna –separating tree and grass responses to environmental cues, J. Veg. Sci., 18(4), 583, doi:10.1111/j.1654-1103.2007.tb02572.x, 2007.

Arora, V. K. and Boer, G. J.: A parameterization of leaf phenology for the terrestrial ecosystem component of climate models, Glob. Chang. Biol., 11(1), 39–59, doi:10.1111/j.1365-2486.2004.00890.x, 2005.

Bacour, C., Peylin, P., MacBean, N., Rayner, P. J., Delage, F., Chevallier, F., Weiss, M., Demarty, J., Santaren, D., Baret, F., Berveiller, D., Dufrêne, E. and Prunet, P.: Joint assimilation of eddy covariance flux measurements and FAPAR products over temperate forests within a process-oriented biosphere model, J. Geophys. Res. Biogeosciences, 120, 1–19, doi:10.1002/2015JG002966, 2015.

Badeck, F. W., Bondeau, A., Böttcher, K., Doktor, D., Lucht, W., Schaber, J. and Sitch, S.: Responses of spring phenology to climate change, New Phytol., 162(2), 295–309, doi:10.1111/j.1469-8137.2004.01059.x, 2004.

Barichivich, J., Briffa, K. R., Myneni, R. B., Osborn, T. J., Melvin, T. M., Ciais, P., Piao, S. and Tucker, C.: Large-scale variations in the vegetation growing season and annual cycle of atmospheric CO2 at high northern latitudes from 1950 to 2011, Glob. Chang. Biol., 19(10), 3167–3183, doi:10.1111/gcb.12283, 2013.

Blümel, K. and Chmielewski, F. M.: Shortcomings of classical phenological forcing models and a way to overcome them, Agric. For. Meteorol., 164, 10–19, doi:10.1016/j.agrformet.2012.05.001, 2012.

Botta, a, Viovy, N., Ciais, P., Friedlingstein, P. and Monfray, P.: A global prognostic scheme of vegetation growth onset using satellite data, Glob. Chang. Biol., 6(7), 709–725, 2000.

Caldararu, S., Purves, D. W. and Palmer, P. I.: Phenology as a strategy for carbon optimality: A global model, Biogeosciences, 11(3), 763–778, doi:10.5194/bg-11-763-2014, 2014.

Choler, P., Sea, W., Briggs, P., Raupach, M. and Leuning, R.: A simple ecohydrological model captures essentials of seasonal leaf dynamics in semi-arid tropical grasslands, Biogeosciences, 7, 907–920, doi:10.5194/bgd-6-8661-2009, 2010.

Chuine, I.: A unified model for budburst of trees., J. Theor. Biol., 207(3), 337–347, doi:10.1006/jtbi.2000.2178, 2000.

33

Chuine, I., Cour, P. and Rousseau, D. D.: Fitting models predicting dates of flowering of temperate-zone trees using simulated annealing, Plant, Cell Environ., 21(5), 455–466, doi:10.1046/j.1365-3040.1998.00299.x, 1998.

Chuine, I., Cambon, G. and Comtois, P.: Scaling phenology from the local to the regional level: Advances from species-specific phenological models, Glob. Chang. Biol., 6(8), 943–952, doi:10.1046/j.1365-2486.2000.00368.x, 2000.

Ciais, P., Sabine, C., Bala, G., Bopp, L., Brovkin, V., Canadell, J., Chhabra, A., DeFries, R., Galloway, J., Heimann, M., Jones, C., Le Quéré, C., Myneny, R. B., Piao, S. and Thornton, P.: Carbon and Other Biogeochemical Cycles, Clim. Chang. 2013 Phys. Sci. Basis. Contrib. Work. Gr. I to Fifth Assess. Rep. Intergov. Panel Clim. Chang., 465–570, doi:10.1017/CBO9781107415324.014, 2013.

Cleland, E. E., Chuine, I., Menzel, A., Mooney, H. a. and Schwartz, M. D.: Shifting plant phenology in response to global change, Trends Ecol. Evol., 22(7), 357–365, doi:10.1016/j.tree.2007.04.003, 2007.

Collatz, G. J., Ribas-Carbo, M. and Berry, J. a.: Coupled photosynthesis-stomatal conductance model for leaves of C4 plants, Aust. J. Plant Physiol., 19(5), 519–539, doi:10.1071/PP9920519, 1992.

D'Odorico, P., Gonsamo, A., Pinty, B., Gobron, N., Coops, N., Mendez, E. and Schaepman, M. E.: Intercomparison of fraction of absorbed photosynthetically active radiation products derived from satellite data over Europe, Remote Sens. Environ., 142, 141–154, doi:10.1016/j.rse.2013.12.005, 2014.

Dardel, C., Kergoat, L., Hiernaux, P., Mougin, E., Grippa, M. and Tucker, C. J.: Re-greening Sahel: 30 years of remote sensing data and field observations (Mali, Niger), Remote Sens. Environ., 140, 350–364, doi:10.1016/j.rse.2013.09.011, 2014.

Dee, D. P., Uppala, S. M., Simmons, a. J., Berrisford, P., Poli, P., Kobayashi, S., Andrae, U., Balmaseda, M. a., Balsamo, G., Bauer, P., Bechtold, P., Beljaars, a. C. M., van de Berg, L., Bidlot, J., Bormann, N., Delsol, C., Dragani, R., Fuentes, M., Geer, a. J., Haimberger, L., Healy, S. B., Hersbach, H., Hólm, E. V., Isaksen, L., Kållberg, P., Köhler, M., Matricardi, M., Mcnally, a. P., Monge-Sanz, B. M., Morcrette, J. J., Park, B. K., Peubey, C., de Rosnay, P., Tavolato, C., Thépaut, J. N. and Vitart, F.: The ERA-Interim reanalysis: Configuration and performance of the data assimilation system, Q. J. R. Meteorol. Soc., 137(656), 553–597, doi:10.1002/qj.828, 2011.

Delbart, N., Picard, G., Le Toan, T., Kergoat, L., Quegan, S., Woodward, I., Dye, D. and Fedotova, V.: Spring phenology in boreal Eurasia over a nearly century time scale, Glob. Chang. Biol., 14(3), 603–614, doi:10.1111/j.1365-2486.2007.01505.x, 2008.

Do, F. C., Goudiaby, V. a., Gimenez, O., Diagne, A. L., Diouf, M., Rocheteau, A. and Akpo, L. E.: Environmental influence on canopy phenology in the dry tropics, For. Ecol. Manage., 215(1-3), 319–328, doi:10.1016/j.foreco.2005.05.022, 2005.

34

1 Dragoni, D., Schmid, H. P., Wayson, C. a., Potter, H., Grimmond, C. S. B. and Randolph, J.
2 C.: Evidence of increased net ecosystem productivity associated with a longer vegetated
3 season in a deciduous forest in south-central Indiana, USA, Glob. Chang. Biol., 17(2), 886–
4 897, doi:10.1111/j.1365-2486.2010.02281.x, 2011.

5 Dufresne, J. L., Foujols, M. a., Denvil, S., Caubel, a., Marti, O., Aumont, O., Balkanski, Y.,
6 Bekki, S., Bellenger, H., Benshila, R., Bony, S., Bopp, L., Braconnot, P., Brockmann, P.,
7 Cadule, P., Cheruy, F., Codron, F., Cozic, a., Cugnet, D., de Noblet, N., Duvel, J. P., Ethé, C.,
8 Fairhead, L., Fichefet, T., Flavoni, S., Friedlingstein, P., Grandpeix, J. Y., Guez, L.,
9 Guilyardi, E., Hauglustaine, D., Hourdin, F., Idelkadi, a., Ghattas, J., Joussaume, S.,
10 Kageyama, M., Krinner, G., Labetoulle, S., Lahellec, a., Lefebvre, M. P., Lefevre, F., Levy,
11 C., Li, Z. X., Lloyd, J., Lott, F., Madec, G., Mancip, M., Marchand, M., Masson, S.,
12 Meurdesoif, Y., Mignot, J., Musat, I., Parouty, S., Polcher, J., Rio, C., Schulz, M.,
13 Swingedouw, D., Szopa, S., Talandier, C., Terray, P., Viovy, N. and Vuichard, N.: Climate
14 change projections using the IPSL-CM5 Earth System Model: From CMIP3 to CMIP5., 2013.

15 Enting, I. G., Rayner, P. J. and Ciais, P.: Carbon cycle uncertainty in regional carbon cycle
16 assessment and processes (RECCAP), Biogeosciences, 9(8), 2889–2904, doi:10.5194/bg-9-
17 2889-2012, 2012.

18 Farquhar, G. D., Caemmerer, S. Von and Berry, J. a: A Biochemical Model of Photosynthetic
19 CO_2 Assimilation in Leaves of C3 Species, Planta, 149, 78–90, 1980.

20 Fensholt, R., Sandholt, I. and Rasmussen, M. S.: Evaluation of MODIS LAI, fAPAR and the
21 relation between fAPAR and NDVI in a semi-arid environment using in situ measurements,
22 Remote Sens. Environ., 91(3-4), 490–507, doi:10.1016/j.rse.2004.04.009, 2004.

23 Fensholt, R., Langanke, T., Rasmussen, K., Reenberg, A., Prince, S. D., Tucker, C., Scholes,
24 R. J., Le, Q. B., Bondeau, A., Eastman, R., Epstein, H., Gaughan, A. E., Hellden, U., Mbow,
25 C., Olsson, L., Paruelo, J., Schweitzer, C., Seaquist, J. and Wessels, K.: Greenness in semi-
26 arid areas across the globe 1981-2007 - an Earth Observing Satellite based analysis of trends
27 and drivers, Remote Sens. Environ., 121, 144–158, doi:10.1016/j.rse.2012.01.017, 2012.

28 Fisher, J. I. and Mustard, J. F.: Cross-scalar satellite phenology from ground, Landsat, and
29 MODIS data, Remote Sens. Environ., 109(3), 261–273, doi:10.1016/j.rse.2007.01.004, 2007.

30 Forkel, M., Carvalhais, N., Schaphoff, S., v. Bloh, W., Migliavacca, M., Thurner, M. and
31 Thonicke, K.: Identifying environmental controls on vegetation greenness phenology through
32 model-data integration, Biogeosciences, 11, 7025–2050, doi:10.5194/bgd-11-7025-2014,
33 2014.

34 Friedlingstein, P., Joel, G., Field, C. B. and Fung, I. Y.: Toward an allocation scheme for
35 global terrestrial carbon models, Glob. Chang. Biol., 5, 755–770, 1999.

36 Fu, Y. H., Campioli, M., Van Oijen, M., Deckmyn, G. and Janssens, I. a.: Bayesian
37 comparison of six different temperature-based budburst models for four temperate tree
38 species, Ecol. Modell., 230, 92–100, doi:10.1016/j.ecolmodel.2012.01.010, 2012.

35

Galvagno, M., Rossini, M., Migliavacca, M., Cremonese, E., Colombo, R. and Morra di Cella, U.: Seasonal course of photosynthetic efficiency in Larix decidua Mill. in response to temperature and change in pigment composition during senescence, Int. J. Biometeorol., 57(6), 871–880, doi:10.1007/s00484-012-0614-y, 2013.

Garrigues, S., Lacaze, R., Baret, F., Morisette, J. T., Weiss, M., Nickeson, J. E., Fernandes, R., Plummer, S., Shabanov, N. V., Myneni, R. B., Knyazikhin, Y. and Yang, W.: Validation and intercomparison of global Leaf Area Index products derived from remote sensing data, J. Geophys. Res. Biogeosciences, 113(2), doi:10.1029/2007JG000635, 2008.

Hänninen, H. and Kramer, K.: A framework for modelling the annual cycle of trees in boreal and temperate regions, Silva Fenn., 41(1), 167–205, 2007.

Hänninen, H. and Tanino, K.: Tree seasonality in a warming climate, Trends Plant Sci., 16(8), 412–416, doi:10.1016/j.tplants.2011.05.001, 2011.

Hickler, T., Eklundh, L., Seaquist, J. W., Smith, B., Ardö, J., Olsson, L., Sykes, M. T. and Sjöström, M.: Precipitation controls Sahel greening trend, Geophys. Res. Lett., 32(21), 1–4, doi:10.1029/2005GL024370, 2005.

Hunter, A. F. and Lechowicz, M. J.: Predicting the Timing of Budburst in Temperate Trees, J. Appl. Ecol., 29(3), 597–604, 1992.

Jeong, S. J., Ho, C. H., Gim, H. J. and Brown, M. E.: Phenology shifts at start vs. end of growing season in temperate vegetation over the Northern Hemisphere for the period 1982-2008, Glob. Chang. Biol., 17(7), 2385–2399, doi:10.1111/j.1365-2486.2011.02397.x, 2011.

Jeong, S. J., Medvigy, D., Shevliakova, E. and Malyshev, S.: Uncertainties in terrestrial carbon budgets related to spring phenology, J. Geophys. Res. Biogeosciences, 117(1), 1–17, doi:10.1029/2011JG001868, 2012.

Jung, M., Reichstein, M. and Bondeau, a.: Towards global empirical upscaling of FLUXNET eddy covariance observations: validation of a model tree ensemble approach using a biosphere model, Biogeosciences Discuss., 6(3), 5271–5304, doi:10.5194/bgd-6-5271-2009, 2009.

Jung, M., Reichstein, M., Margolis, H. a., Cescatti, A., Richardson, A. D., Arain, M. A., Arneth, A., Bernhofer, C., Bonal, D., Chen, J., Gianelle, D., Gobron, N., Kiely, G., Kutsch, W., Lasslop, G., Law, B. E., Lindroth, A., Merbold, L., Montagnani, L., Moors, E. J., Papale, D., Sottocornola, M., Vaccari, F. and Williams, C.: Global patterns of land-atmosphere fluxes of carbon dioxide, latent heat, and sensible heat derived from eddy covariance, satellite, and meteorological observations, J. Geophys. Res. Biogeosciences, 116(3), 2–4, doi:10.1029/2010JG001566, 2011.

Kattge, J., Díaz, S., Lavorel, S., Prentice, I. C., Leadley, P., Bönisch, G., Garnier, E., Westoby, M., Reich, P. B., Wright, I. J., Cornelissen, J. H. C., Violle, C., Harrison, S. P., Van Bodegom, P. M., Reichstein, M., Enquist, B. J., Soudzilovskaia, N. a., Ackerly, D. D., Anand, M., Atkin, O., Bahn, M., Baker, T. R., Baldocchi, D., Bekker, R., Blanco, C. C., Blonder, B., Bond, W. J., Bradstock, R., Bunker, D. E., Casanoves, F., Cavender-Bares, J., Chambers, J.

Q., Chapin, F. S., Chave, J., Coomes, D., Cornwell, W. K., Craine, J. M., Dobrin, B. H., Duarte, L., Durka, W., Elser, J., Esser, G., Estiarte, M., Fagan, W. F., Fang, J., Fernández-Méndez, F., Fidelis, a., Finegan, B., Flores, O., Ford, H., Frank, D., Freschet, G. T., Fyllas, N. M., Gallagher, R. V., Green, W. a., Gutierrez, a. G., Hickler, T., Higgins, S. I., Hodgson, J. G., Jalili, a., Jansen, S., Joly, C. a., Kerkhoff, a. J., Kirkup, D., Kitajima, K., Kleyer, M., Klotz, S., Knops, J. M. H., Kramer, K., Kühn, I., Kurokawa, H., Laughlin, D., Lee, T. D., Leishman, M., Lens, F., Lenz, T., Lewis, S. L., Lloyd, J., Llusià, J., Louault, F., Ma, S., Mahecha, M. D., Manning, P., Massad, T., Medlyn, B. E., Messier, J., Moles, a. T., Müller, S. C., Nadrowski, K., Naeem, S., Niinemets, Ü., Nöllert, S., Nüske, a., Ogaya, R., Oleksyn, J., Onipchenko, V. G., Onoda, Y., Ordoñez, J., Overbeck, G., et al.: TRY - a global database of plant traits, Glob. Chang. Biol., 17(9), 2905–2935, doi:10.1111/j.1365-2486.2011.02451.x, 2011.

Keenan, T., Gray, J. and Friedl, M.: Net carbon uptake has increased through warming-induced changes in temperate forest phenology, Nat. Clim. Chang., 4(June), 598–604, doi:10.1038/NCLIMATE2253, 2014.

Keenan, T. F., Baker, I., Barr, A., Ciais, P., Davis, K., Dietze, M., Dragoni, D., Gough, C. M., Grant, R., Hollinger, D., Hufkens, K., Poulter, B., Mccaughey, H., Raczka, B., Ryu, Y., Schaefer, K., Tian, H., Verbeeck, H., Zhao, M. and Richardson, A. D.: Terrestrial biosphere model performance for inter-annual variability of land-atmosphere CO 2 exchange, Glob. Chang. Biol., 18(6), 1971–1987, doi:10.1111/j.1365-2486.2012.02678.x, 2012.

Kim, Y. and Wang, G.: Modeling seasonal vegetation variation and its validation against Moderate Resolution Imaging Spectroradiometer (MODIS) observations over North America, J. Geophys. Res. D Atmos., 110(4), 1–13, doi:10.1029/2004JD005436, 2005.

Knorr, W., Kaminski, T., Scholze, M., Gobron, N., Pinty, B., Giering, R. and Mathieu, P. P.: Carbon cycle data assimilation with a generic phenology model, J. Geophys. Res. Biogeosciences, 115(4), 1–16, doi:10.1029/2009JG001119, 2010.

Knyazikhin, Y., Martonchik, J. V., Myneni, R. B., Diner, D. J. and Running, S. W.: Synergistic algorithm for estimating vegetation canopy leaf area index and fraction of absorbed photosynthetically active radiation from MODIS and MISR data, J. Geophys. Res., 103(D24), 32257, doi:10.1029/98JD02462, 1998.

Körner, C. and Basler, D.: Plant science. Phenology under global warming., Science, 327(5972), 1461–1462, doi:10.1126/science.1186473, 2010.

Kovalskyy, V. and Henebry, G. M.: A new concept for simulation of vegetated land surface dynamics-Part 1: The event driven phenology model, Biogeosciences, 9(1), 141–159, doi:10.5194/bg-9-141-2012, 2012a.

Kovalskyy, V. and Henebry, G. M.: Alternative methods to predict actual evapotranspiration illustrate the importance of accounting for phenology-Part 2: The event driven phenology model, Biogeosciences, 9(1), 161–177, doi:10.5194/bg-9-161-2012, 2012b.

Krinner, G., Viovy, N., de Noblet-Ducoudré, N., Ogée, J., Polcher, J., Friedlingstein, P., Ciais, P., Sitch, S. and Prentice, I. C.: A dynamic global vegetation model for studies of the

37

1   coupled atmosphere-biosphere system, Global Biogeochem. Cycles, 19(1), 1–33,
2   doi:10.1029/2003GB002199, 2005.

3   Kucharik, C. J., Barford, C. C., Maayar, M. El, Wofsy, S. C., Monson, R. K. and Baldocchi,
4   D. D.: A multiyear evaluation of a Dynamic Global Vegetation Model at three AmeriFlux
5   forest sites: Vegetation structure, phenology, soil temperature, and CO2 and H2O vapor
6   exchange, Ecol. Modell., 196(1-2), 1–31, doi:10.1016/j.ecolmodel.2005.11.031, 2006.

7   Kuppel, S., Peylin, P., Chevallier, F., Bacour, C., Maignan, F. and Richardson, a. D.:
8   Constraining a global ecosystem model with multi-site eddy-covariance data, Biogeosciences,
9   9(10), 3757–3776, doi:10.5194/bg-9-3757-2012, 2012.

10   Kuppel, S., Peylin, P., Maignan, F., Chevallier, F., Kiely, G., Montagnani, L. and Cescatti, a.:
11   Model–data fusion across ecosystems: from multi-site optimizations to global simulations,
12   Geosci. Model Dev. Discuss., 7(3), 2961–3011, doi:10.5194/gmdd-7-2961-2014, 2014.

13   Lafont, S., Zhao, Y., Calvet, J. C., Peylin, P., Ciais, P., Maignan, F. and Weiss, M.: Modelling
14   LAI, surface water and carbon fluxes at high-resolution over France: Comparison of ISBA-A-
15   gs and ORCHIDEE, Biogeosciences, 9(1), 439–456, doi:10.5194/bg-9-439-2012, 2012.

16   Levis, S. and Bonan, G. B.: Simulating springtime temperature patterns in the community
17   atmosphere model coupled to the community land model using prognostic leaf area, J. Clim.,
18   17(23), 4531–4540, doi:10.1175/3218.1, 2004.

19   Linkosalo, T., Lappalainen, H. K. and Hari, P.: A comparison of phenological models of leaf
20   bud burst and flowering of boreal trees using independent observations., Tree Physiol.,
21   28(12), 1873–1882, doi:10.1093/treephys/28.12.1873, 2008.

22   Maignan, F., Bréon, F. M., Bacour, C., Demarty, J. and Poirson, a.: Interannual vegetation
23   phenology estimates from global AVHRR measurements. Comparison with in situ data and
24   applications, Remote Sens. Environ., 112(2), 496–505, doi:10.1016/j.rse.2007.05.011, 2008.

25   Maignan, F., Bréon, F.-M., Chevallier, F., Viovy, N., Ciais, P., Garrec, C., Trules, J. and
26   Mancip, M.: Evaluation of a Global Vegetation Model using time series of satellite vegetation
27   indices, Geosci. Model Dev., 4(4), 1103–1114, doi:10.5194/gmd-4-1103-2011, 2011.

28   Melaas, E. K., Richardson, A. D., Friedl, M. a., Dragoni, D., Gough, C. M., Herbst, M.,
29   Montagnani, L. and Moors, E.: Using FLUXNET data to improve models of springtime
30   vegetation activity onset in forest ecosystems, Agric. For. Meteorol., 171-172, 46–56,
31   doi:10.1016/j.agrformet.2012.11.018, 2013.

32   Migliavacca, M., Galvagno, M., Cremonese, E., Rossini, M., Meroni, M., Sonnentag, O.,
33   Cogliati, S., Manca, G., Diotri, F., Busetto, L., Cescatti, A., Colombo, R., Fava, F., Morra di
34   Cella, U., Pari, E., Siniscalco, C. and Richardson, A. D.: Using digital repeat photography and
35   eddy covariance data to model grassland phenology and photosynthetic CO2 uptake, Agric.
36   For. Meteorol., 151(10), 1325–1337, doi:10.1016/j.agrformet.2011.05.012, 2011.

37   Migliavacca, M., Sonnentag, O., Keenan, T. F., Cescatti, a., O'Keefe, J. and Richardson, a.
38   D.: On the uncertainty of phenological responses to climate change, and implications for a

38

terrestrial biosphere model, Biogeosciences, 9(6), 2063–2083, doi:10.5194/bg-9-2063-2012, 2012.

Morisette, J. T., Richardson, A. D., Knapp, A. K., Fisher, J. I., Graham, E. a., Abatzoglou, J., Wilson, B. E., Breshears, D. D., Henebry, G. M., Hanes, J. M. and Liang, L.: Tracking the rhythm of the seasons in the face of global change: Phenological research in the 21 st century, Front. Ecol. Environ., 7(5), 253–260, doi:10.1890/070217, 2009.

Murray-Tortarolo, G., Anav, A., Friedlingstein, P., Sitch, S., Piao, S., Zhu, Z., Poulter, B., Zaehle, S., Ahlström, A., Lomas, M., Levis, S., Viovy, N. and Zeng, N.: Evaluation of land surface models in reproducing satellite-derived LAI over the high-latitude northern hemisphere. Part I: Uncoupled DGVMs, Remote Sens., 5(10), 4819–4838, doi:10.3390/rs5104819, 2013.

Myneni, R. B. and Williams, D. L.: On the relationship between FAPAR and NDVI, Remote Sens. Environ., 49(3), 200–211, doi:10.1016/0034-4257(94)90016-7, 1994.

Myneni, R. B., Keeling, C. D., Tucker, C. J., Asrar, G. and Nemani, R. R.: Increased plant growth in the northern high latitudes from 1981 to 1991, Nature, 386, 698–702, 1997.

Naudts, K., Ryder, J., McGrath, M. J., Otto, J., Chen, Y., Valade, a., Bellasen, V., Berhongaray, G., Bönisch, G., Campioli, M., Ghattas, J., De Groote, T., Haverd, V., Kattge, J., MacBean, N., Maignan, F., Merilä, P., Penuelas, J., Peylin, P., Pinty, B., Pretzsch, H., Schulze, E. D., Solyga, D., Vuichard, N., Yan, Y. and Luyssaert, S.: A vertically discretised canopy description for ORCHIDEE (SVN r2290) and the modifications to the energy, water and carbon fluxes, Geosci. Model Dev., 8(7), 2035–2065, doi:10.5194/gmd-8-2035-2015, 2015.

O'Hagan, A.: Eliciting Expert Beliefs in Substantial Practical Applications, Stat., 47, 21–35, 1998.

O'Hagan, A.: Probabilistic uncertainty specification: Overview, elaboration techniques and their application to a mechanistic model of carbon flux, Environ. Model. Softw., 36, 35–48, doi:10.1016/j.envsoft.2011.03.003, 2012.

Olsson, C., Bolmgren, K., Lindström, J. and Jönsson, A. M.: Performance of tree phenology models along a bioclimatic gradient in Sweden, Ecol. Modell., 266(1), 103–117, doi:10.1016/j.ecolmodel.2013.06.026, 2013.

Orlandi, F., Garcia-Mozo, H., Vazquez Ezquerra, L., Romano, B., Dominguez, E., Galan, C. and Fornaciari, M.: Phenological chilling requirements in Umbria (Italy) and Andalusia (Spain), Plant Biosyst., 138, 111–116, 2004.

Parmesan, C.: Influences of species, latitudes and methodologies on estimates of phenological response to global warming, Glob. Chang. Biol., 13(9), 1860–1872, doi:10.1111/j.1365-2486.2007.01404.x, 2007.

Peñuelas, J., Rutishauser, T. and Filella, I.: Ecology. Phenology feedbacks on climate change., Science, 324(5929), 887–888, doi:10.1126/science.1173004, 2009.

39

Piao, S., Friedlingstein, P., Ciais, P., Zhou, L. and Chen, A.: Effect of climate and CO2 changes on the greening of the Northern Hemisphere over the past two decades, Geophys. Res. Lett., 33(23), 2–7, doi:10.1029/2006GL028205, 2006.

Piao, S., Friedlingstein, P., Ciais, P., Viovy, N. and Demarty, J.: Growing season extension and its impact on terrestrial carbon cycle in the Northern Hemisphere over the past 2 decades, Global Biogeochem. Cycles, 21(3), 1–11, doi:10.1029/2006GB002888, 2007.

Piao, S., Ciais, P., Friedlingstein, P., Peylin, P., Reichstein, M., Luyssaert, S., Margolis, H., Fang, J., Barr, A., Chen, A., Grelle, A., Hollinger, D. Y., Laurila, T., Lindroth, A., Richardson, A. D. and Vesala, T.: Net carbon dioxide losses of northern ecosystems in response to autumn warming., Nature, 451(7174), 49–52, doi:10.1038/nature06444, 2008.

Picard, G., Quegan, S., Delbart, N., Lomas, M. R., Le Toan, T. and Woodward, F. I.: Bud-burst modelling in Siberia and its impact on quantifying the carbon budget, Glob. Chang. Biol., 11(12), 2164–2176, doi:10.1111/j.1365-2486.2005.01055.x, 2005.

Pickett-Heaps, C. a., Canadell, J. G., Briggs, P. R., Gobron, N., Haverd, V., Paget, M. J., Pinty, B. and Raupach, M. R.: Evaluation of six satellite-derived Fraction of Absorbed Photosynthetic Active Radiation (FAPAR) products across the Australian continent, Remote Sens. Environ., 140, 241–256, doi:10.1016/j.rse.2013.08.037, 2014.

Rayner, P. J.: The current state of carbon-cycle data assimilation, Curr. Opin. Environ. Sustain., 2(4), 289–296, doi:10.1016/j.cosust.2010.05.005, 2010.

Reich, P. B.: Variation among plant species in leaf turnover rates and associated traits: implications for growth at all life stages, Inherent Var. Plant Growth Physiol. Mech. Ecol. consequences, 467–487, 1998.

Reyer, C. P. O., Leuzinger, S., Rammig, A., Wolf, A., Bartholomeus, R. P., Bonfante, A., de Lorenzi, F., Dury, M., Gloning, P., Abou Jaoudé, R., Klein, T., Kuster, T. M., Martins, M., Niedrist, G., Riccardi, M., Wohlfahrt, G., de Angelis, P., de Dato, G., François, L., Menzel, A. and Pereira, M.: A plant's perspective of extremes: Terrestrial plant responses to changing climatic variability, Glob. Chang. Biol., 19(1), 75–89, doi:10.1111/gcb.12023, 2013.

Reyes-Fox, M., Steltzer, H., Trlica, M. J., McMaster, G. S., Andales, A. a, LeCain, D. R. and Morgan, J. a: Elevated CO2 further lengthens growing season under warming conditions., Nature, 510(7504), 259–62, doi:10.1038/nature13207, 2014.

Richardson, A. D., Hollinger, D. Y., Dail, D. B., Lee, J. T., Munger, J. W. and O'Keefe, J.: Influence of spring phenology on seasonal and annual carbon balance in two contrasting New England forests, Tree Physiol., 29(3), 321–331, doi:10.1093/treephys/tpn040, 2009.

Richardson, A. D., Black, T. A., Ciais, P., Delbart, N., Friedl, M. a, Gobron, N., Hollinger, D. Y., Kutsch, W. L., Longdoz, B., Luyssaert, S., Migliavacca, M., Montagnani, L., Munger, J. W., Moors, E., Piao, S., Rebmann, C., Reichstein, M., Saigusa, N., Tomelleri, E., Vargas, R. and Varlagin, A.: Influence of spring and autumn phenological transitions on forest ecosystem productivity., Philos. Trans. R. Soc. Lond. B. Biol. Sci., 365(1555), 3227–3246, doi:10.1098/rstb.2010.0102, 2010.

1   Richardson, A. D., Anderson, R. S., Arain, M. A., Barr, A. G., Bohrer, G., Chen, G., Chen, J.
2   M., Ciais, P., Davis, K. J., Desai, A. R., Dietze, M. C., Dragoni, D., Garrity, S. R., Gough, C.
3   M., Grant, R., Hollinger, D. Y., Margolis, H. a., Mccaughey, H., Migliavacca, M., Monson,
4   R. K., Munger, J. W., Poulter, B., Raczka, B. M., Ricciuto, D. M., Sahoo, A. K., Schaefer, K.,
5   Tian, H., Vargas, R., Verbeeck, H., Xiao, J. and Xue, Y.: Terrestrial biosphere models need
6   better representation of vegetation phenology: Results from the North American Carbon
7   Program Site Synthesis, Glob. Chang. Biol., 18(2), 566–584, doi:10.1111/j.1365-
8   2486.2011.02562.x, 2012.

9   Richardson, A. D., Keenan, T. F., Migliavacca, M., Ryu, Y., Sonnentag, O. and Toomey, M.:
10   Climate change, phenology, and phenological control of vegetation feedbacks to the climate
11   system, Agric. For. Meteorol., 169, 156–173, doi:10.1016/j.agrformet.2012.09.012, 2013.

12   Rosenthal, S. I. and Camm, E. L.: Photosynthetic decline and pigment loss during autumn
13   foliar senescence in western larch (Larix occidentalis)., Tree Physiol., 17(12), 767–75 [online]
14   Available from: http://www.ncbi.nlm.nih.gov/pubmed/14759886, 1997.

15   Santaren, D., Peylin, P., Viovy, N. and Ciais, P.: Optimizing a process-based ecosystem
16   model with eddy-covariance flux measurements: A pine forest in southern France, Global
17   Biogeochem. Cycles, 21(2), 1–15, doi:10.1029/2006GB002834, 2007.

18   Santaren, D., Peylin, P., Bacour, C., Ciais, P. and Longdoz, B.: Ecosystem model
19   optimization using in-situ flux observations : benefit of monte-carlo vs . variational schemes
20   and analyses of the year-to-year model performances, Biogeosciences, 11, 7137–7158,
21   doi:10.5194/bgd-10-18009-2013, 2014.

22   Schaber, J. and Badeck, F. W.: Physiology-based phenology models for forest tree species in
23   Germany, Int. J. Biometeorol., 47(4), 193–201, doi:10.1007/s00484-003-0171-5, 2003.

24   Stöckli, R., Rutishauser, T., Baker, I., Liniger, M. a. and Denning, a. S.: A global reanalysis
25   of vegetation phenology, J. Geophys. Res. Biogeosciences, 116(3),
26   doi:10.1029/2010JG001545, 2011.

27   Thoning, K. W., Tans, P. P. and Komhyr, W. D.: Atmospheric carbon dioxide at Mauna Loa
28   Observatory: 2. Analysis of the NOAA GMCC data, 1974–1985, J. Geophys. Res., 94(D6),
29   8549, doi:10.1029/JD094iD06p08549, 1989.

30   Traore, A. K., Ciais, P., Vuichard, N., MacBean, N., Jung, M. and Myneni, R.: 1982–2010
31   Trends of Light Use Efficiency and Inherent Water Use Efficiency in African vegetation:
32   Sensitivity to Climate and Atmospheric CO2 Concentrations, Remote Sens., 6, 8923–8944,
33   doi:10.3390/rs6098923, 2014a.

34   Traore, A. K., Ciais, P., Vuichard, N., Poulter, B., Viovy, N., Guimberteau, M., Jung, M.,
35   Myneni, R. and Fisher, J. B.: Evaluation of the ORCHIDEE ecosystem model over Africa
36   against 25 years of satellite-based water and carbon measurements, , 119,
37   doi:10.1002/2014JG002638., 2014b.

41

Vérant, S., Laval, K., Polcher, J. and De Castro, M.: Sensitivity of the Continental Hydrological Cycle to the Spatial Resolution over the Iberian Peninsula, J. Hydrometeorol., 5(2), 267–285, doi:10.1175/1525-7541(2004)005<0267:SOTCHC>2.0.CO;2, 2004.

Verbeeck, H., Peylin, P., Bacour, C., Bonal, D., Steppe, K. and Ciais, P.: fluxes in Amazon forests: Fusion of eddy covariance data and the ORCHIDEE model, J. Geophys. Res., 116(G2), 1–19, doi:10.1029/2010JG001544, 2011.

Vermote, E., Justice, C. O. and Bréon, F. M.: Towards a generalized approach for correction of the BRDF effect in MODIS directional reflectances, IEEE Trans. Geosci. Remote Sens., 47(3), 898–908, doi:10.1109/TGRS.2008.2005977, 2009.

Walker, A. P., Hanson, P. J., De Kauwe, M. G., Medlyn, B. E., Zaehle, S., Asao, S., Dietze, M. C., Hickler, T., Huntingford, C., Iversen, C. M., Jain, A. K., Lomas, M., Luo, Y., Mccarthy, H., Parton, W. J., Prentice, I. C., Thornton, P. E., Wang, S., Wang, Y.-P., Warlind, D., Weng, E., Warren, J. M., Woodward, F. I., Oren, R. and Norby, R.: Comprehensive ecosystem model-data synthesis using multiple data sets at two temperate forest free-air CO2 enrichment experiments: Model performance at ambient CO2 concentration, J. Geophys. Res. Biogeosciences, 119, 937–964, doi:10.1002/2013JG002553, 2014.

White, M. a. and Nemani, R. R.: Canopy duration has little influence on annual carbon storage in the deciduous broad leaf forest, Glob. Chang. Biol., 9(7), 967–972, doi:10.1046/j.1365-2486.2003.00585.x, 2003.

Wolkovich, E. M., Cook, B. I., Allen, J. M., Crimmins, T. M., Betancourt, J. L., Travers, S. E., Pau, S., Regetz, J., Davies, T. J., Kraft, N. J. B., Ault, T. R., Bolmgren, K., Mazer, S. J., McCabe, G. J., McGill, B. J., Parmesan, C., Salamin, N., Schwartz, M. D. and Cleland, E. E.: Warming experiments underpredict plant phenological responses to climate change, Nature, 18–21, doi:10.1038/nature11014, 2012.

Wright, I. J., Reich, P. B., Westoby, M., Ackerly, D. D., Baruch, Z., Bongers, F., Cavender-Bares, J., Chapin, T., Cornelissen, J. H. C., Diemer, M., Flexas, J., Garnier, E., Groom, P. K., Gulias, J., Hikosaka, K., Lamont, B. B., Lee, T., Lee, W., Lusk, C., Midgley, J. J., Navas, M.-L., Niinemets, U., Oleksyn, J., Osada, N., Poorter, H., Poot, P., Prior, L., Pyankov, V. I., Roumet, C., Thomas, S. C., Tjoelker, M. G., Veneklaas, E. J. and Villar, R.: The worldwide leaf economics spectrum., Nature, 428(6985), 821–827, doi:10.1038/nature02403, 2004.

Wullschleger, S. D., Epstein, H. E., Box, E. O., Euskirchen, E. S., Goswami, S., Iversen, C. M., Kattge, J., Norby, R. J., Van Bodegom, P. M. and Xu, X.: Plant functional types in Earth system models: Past experiences and future directions for application of dynamic vegetation models in high-latitude ecosystems, Ann. Bot., 114(1), 1–16, doi:10.1093/aob/mcu077, 2014.

Zobler, L.: A World Soil File for Global Climate Modelling,NASA Technical Memorandum 87802, NASA Goddard Institute for Space Studies, New York, New York, U.S.A, 1986.

Table 1. Standard PFTs used in ORCHIDEE, their short name and corresponding phenology model (see Appendix A for a full description of the phenology models). Evergreen and agriculture PFTs do not have a specific phenology model in the ORCHIDEE TBM.

PFT	Description	Short name	Phenology Model
1	Bare Soil	BS	-
2	Tropical Broadleaved Evergreen	TrBE	-
3	Tropical Broadleaved Raingreen	TrBR	MOI
4	Temperate Needleleaf Evergreen	TeNE	-
5	Temperate Broadleaved Evergreen	TeBE	-
6	Temperate Broadleaved Deciduous	TeBD	NCD_GDD
7	Boreal Needleleaf Evergreen	BoNE	-
8	Boreal Broadleaved Deciduous	BoBD	NCD_GDD
9	Boreal Needleleaf Deciduous	BoND	NGD
10	Natural C3 grass	NC3	MOI_GDD
11	Natural C4 grass	NC4	MOI_GDD
12	C3 crops (agriculture)	AC3	-
13	C4 crops (agriculture)	AC4	-

Table 2: ORCHIDEE parameters optimized. For each PFT the prior values, minimum and maximum values (in squared brackets) and multi-site posterior mean values (in bold) are given. Note the prior uncertainty on the parameters is defined as 40% of the full parameter range.

Parameter	TrBR	TeBD	BoBD	BoND	NC3	NC4
$L_{agecrit}$ (days)	180 [120,240]	180 [90,240]	180 [90,240]	180 [90,240]	120 [60,180]	120 [60,180]
	120	**160.6**	**240**	**90**	**60**	**165.9**
K_{pheno_crit} (-)	-	1.0 [0.7,1.8]	1.0 [0.7,1.8]	1.0 [0.7,1.8]	1.0 [0.7,1.8]	1.0 [0.7,1.8]
		1.13	**0.87**	**1.1**	**0.77**	**0.9**
K_{lai_happy} (-)	0.5 [0.35,0.7]	0.5 [0.35,0.7]	0.5 [0.35,0.7]	0.5 [0.35,0.7]	0.5 [0.35,0.7]	0.5 [0.35,0.7]
	0.7	**0.4**	**0.36**	**0.35**	**0.35**	**0.47**
T_{senes} (^oC)	-	12.0 [2,22]	7.0 [-3,17]	2.0 [-8,12]	-1.375 [-11.38,9.38]	5.0 [-1,11]
		16.6	**14.6**	**12**	**9.375**	**0.85**
L_{fall} (-)	10.0 [2,50]	10.0 [2,50]	10.0 [2,50]	10.0 [2,50]	-	-
	10.0	**29.5**	**4.7**	**9.0**		
$Moist_{Tmin}$ (days)	50 [10,100]	-	-	-	35.0 [5,70]	35.0 [5,70]
	10				**36.4**	**55.95**
$Moist_{senes, no\_senes}$ (-)	0.3 [0.2,0.8]	-	-	-	-	-
	-	-	-	-	0.3 [0.25,0.7]	0.3 [0.25,0.7]
	0.8				**0.65**	**0.39**

Table 3: Metrics to describe the ability of the optimization algorithm to find the global minimum of the cost function for the MS optimization using 20 twenty different random "first guess" parameters. The 2nd column shows the final value (after 25 iterations of the BFGS optimizer) for the random test that resulted in the lowest value of $J(x)$ (the cost function), which corresponds to the highest % reduction in $J(x)$. The 3rd column gives an indication of the distribution of the final values for all 20 tests with respect to the lowest value obtained (given in column 1). This is represented as the difference between the final value of $J(x)$ for each test and the minimum value of $J(x)$, divided by the same minimum value. The 4th column shows the % reduction of $J(x)$ normalized to the value of $J(x)$ for the default parameters of ORCHIDEE. The two values for the 3rd and 4th columns represent the interquartile range (25th to 75th percentiles) for the spread across the 20 random tests.

PFT	Minimum $J(x)$	Fractional Difference from J_{min}	% Reduction (J/J_b)
TrBR	9720	0.24 – 0.25	44.1 – 44.6
TeBD	4730	0.2 – 0.5	28 – 44
BoBD	4260	0.07 – 0.32	54 – 63
BoND	2000	0.02 – 0.31	77 – 82
NC3	6590	0.08 – 0.34	29 – 44
NC4	19160	0.03 – 0.1	4 – 11

45

Table 4: Prior and posterior median (across sites) RMSE and R (and median reduction of RMSE in % in brackets) for the fifteen sites included in the optimization and for the fifteen sites used for spatial validation, for each PFT. For the temporal validation all thirty sites are included, but only for the 2009-2010 period. For the spatial and temporal validation, the posterior MS parameter vector was used.

PFT	Optimization						Spatial validation				Temporal Validation			
	Prior RMSE	SS Post RMSE	MS Post RMSE	Prior R	SS Post. R	MS Post. R	Prior RMSE	Post RMSE	Prior R	Post. R	Prior RMSE	Post RMSE	Prior R	Post. R
TrBR	0.29	0.18 (39)	0.22 (24)	0.73	0.87	0.82	0.28	0.18 (32)	0.76	0.88	0.28	0.18 (33)	0.75	0.88
TeBD	0.20	0.12 (39)	0.16 (21)	0.90	0.97	0.93	0.20	0.16 (19)	0.91	0.94	0.20	0.17 (18)	0.92	0.94
BoBD	0.30	0.14 (57)	0.14 (52)	0.54	0.91	0.91	0.29	0.15 (47)	0.59	0.89	0.31	0.23 (26)	0.56	0.67
BoND	0.39	0.15 (61)	0.16 (57)	0.41	0.90	0.89	0.38	0.16 (59)	0.42	0.90	0.39	0.16 (58)	0.40	0.88
NC3	0.31	0.20 (34)	0.20 (32)	0.62	0.82	0.85	0.30	0.22 (26)	0.65	0.77	0.31	0.21 (35)	0.61	0.79
NC4	0.23	0.21 (11)	0.24 (0)	0.81	0.82	0.81	0.24	0.23 (7)	0.75	0.79	0.24	0.23 (3)	0.80	0.86

1 Table 5: Median prior and posterior correlation between modelled fAPAR and satellite NDVI

2 daily time series and inter-annual anomalies of the annual mean. The metrics are computed

3 for each PFT for grid cells that contained >= fraction that was used to select the sites for the

4 PFT in question (see Section 2.3.3).

5

PFT	Time series correlation		IAV correlation	
	Prior	Posterior	Prior	Posterior
TrBE	0.18	0.19	0.21	0.13
TrBR	0.71	0.85	0.31	0.29
TeNE	0.29	0.44	0.30	0.42
TeBE	0.32	0.19	0.54	0.44
TeBD	0.88	0.89	0.30	0.44
BoNE	0.35	0.45	0.25	0.22
BoBD	0.52	0.86	0.48	0.40
BoND	0.33	0.81	0.02	0.13
NC3	0.56	0.76	0.29	0.32
NC4	0.70	0.74	0.30	0.30
AC3	0.36	0.35	0.49	0.50
AC4	0.48	0.48	0.33	0.35

6

7

8

9

Table 6: Median prior and posterior bias between model- and observation-derived Start Of Season (SOS) and End Of Season (EOS) dates (model – observations). The metrics are computed for each PFT for grid cells that contained >= fraction that was used to select the sites for the PFT in question (see Section 2.3.3). A negative bias indicates the modelled date is earlier than the one calculated from the observations.

PFT	SOS bias		EOS bias	
	Prior	Posterior	Prior	Posterior
TrBE	20	-3	-146	-3
TrBR	30	13	9	12
TeNE	38	20	41	-33
TeBE	70	49	42	-4
TeBD	4	6	14	13
BoNE	38	29	52	13
BoBD	18	10	43	8
BoND	5	1	36	2
NC3	25	15	42	-1
NC4	32	15	-7	-2
AC3	-17	-17	19	18
AC4	8	8	18	18
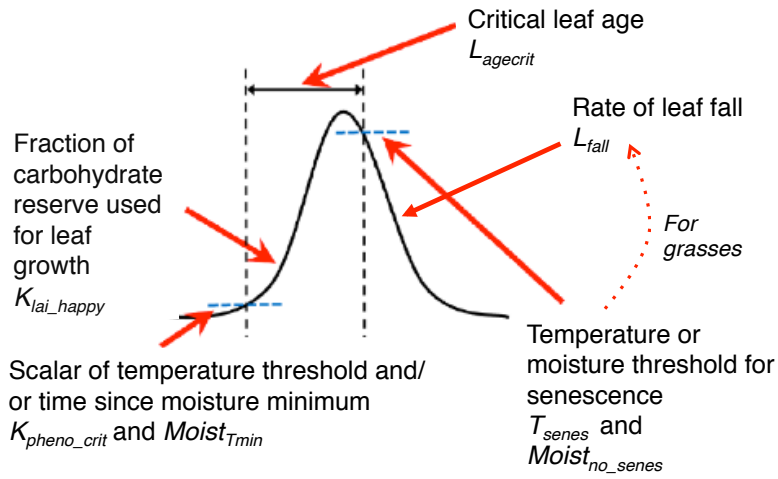
Figure 1: Schematic to show how the optimized parameters control the timing of the leaf phenology in ORCHIDEE. The dotted arrow shows that the temperature and moisture threshold for senescence also affects the rate of leaf fall for grasses by slowing down the turnover rate once this threshold has been reached (whereas for trees only the L_{fall} parameter is used).

1

2

3

4

5

6

7

8

9

10

11
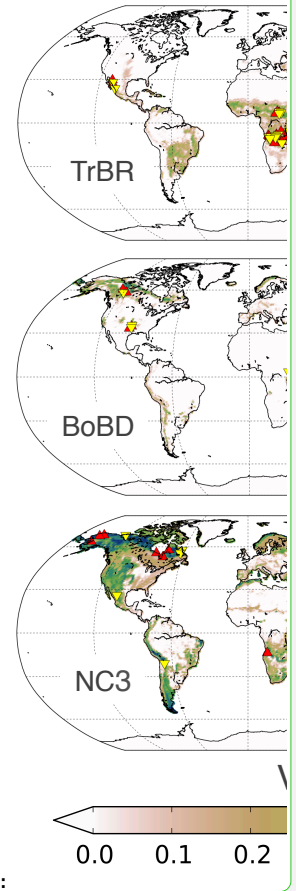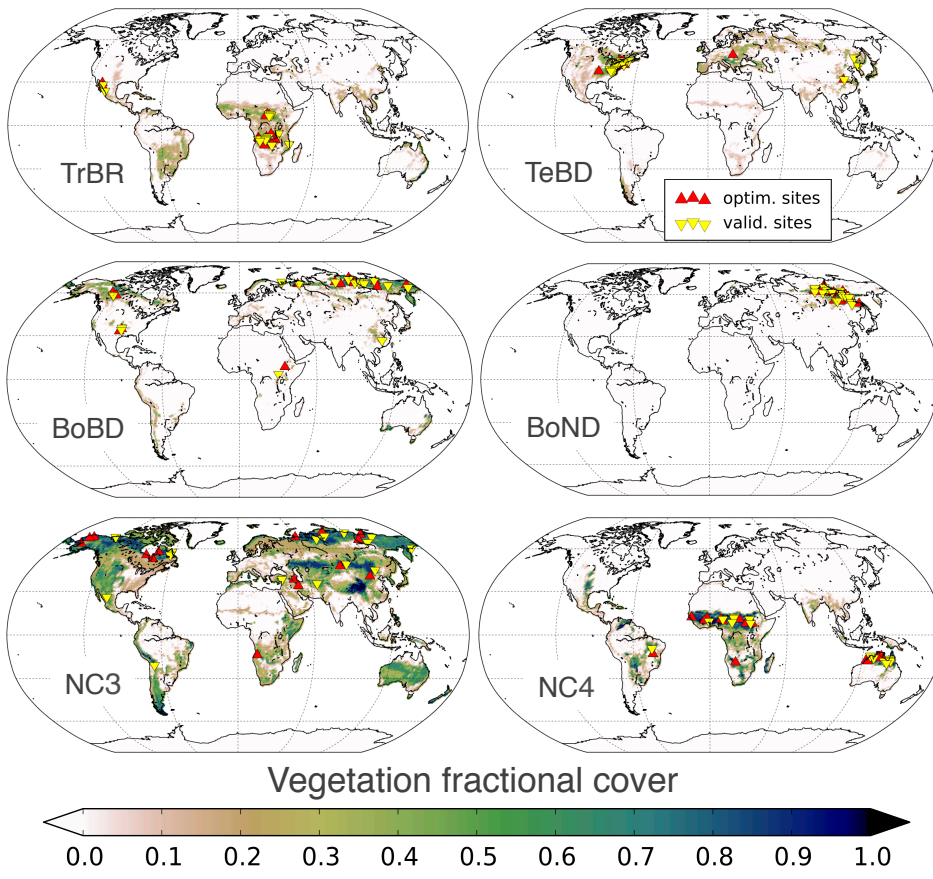
Figure 2: Global distributions of fractional cover for the six PFTs optimized in this study. Red upright triangles mark the location of the optimization sites, and yellow upside-down triangles mark the location of the validation sites.

50
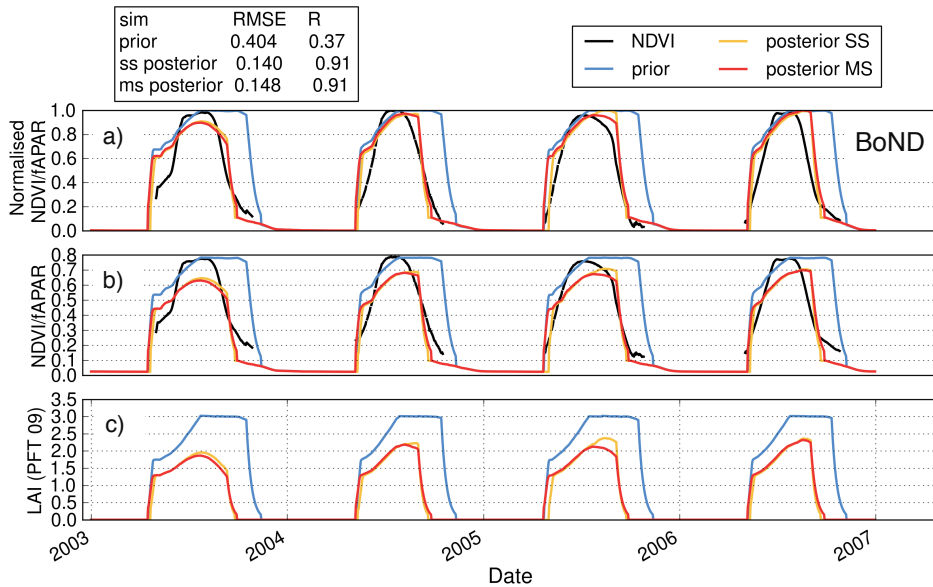
Figure 3: Time-series (zoom to 2003 – 2007) for one example BoND PFT site (72°N, 120.24°E) of a) the normalized modelled total fAPAR and MODIS NDVI data; b) the un-scaled model total fAPAR and MODIS NDVI data; c) the corresponding modelled LAI for the BoND PFT only. The black curve corresponds to the MODIS NDVI data, the blue curve is the prior model simulation, the orange curve shows the model simulation using the posterior parameters from the SS optimization, and the red curve corresponds to the model simulation at this site using the MS posterior parameter values. The prior and posterior RMSE and R are given in the upper left box. The MODIS NDVI and model fAPAR time series were normalized to their maximum and minimum value over the 2000 – 2008 period for the optimization (see Section 2.2.1).

51
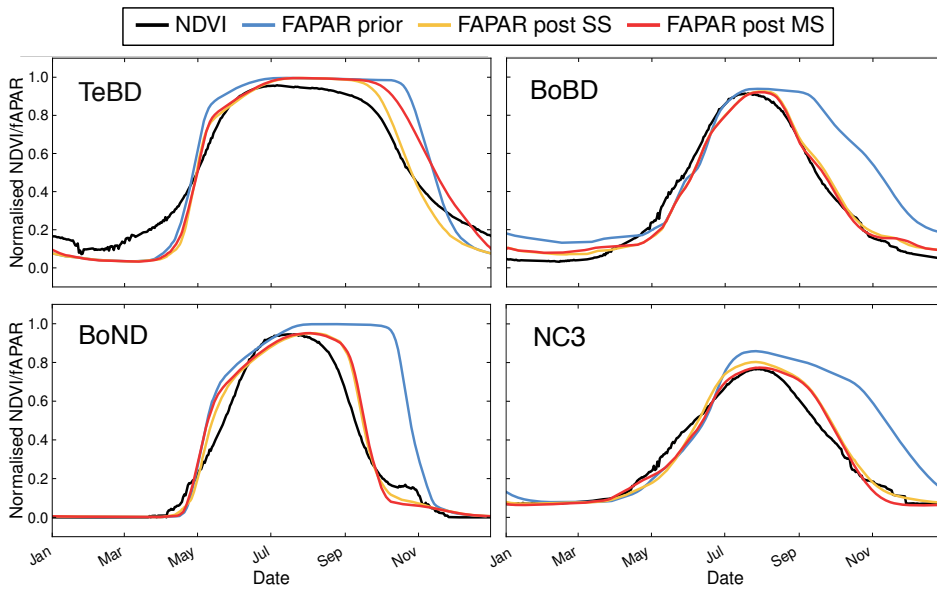
Figure 4: The mean seasonal cycle of the normalized modelled fAPAR before and after optimization, compared to that of the MODIS NDVI data, for the temperate and boreal deciduous PFTs (TeBD, BoBD, BoND and NC3). Black = MODIS NDVI data; blue = prior model; orange = single-site optimization; red = multi-site optimization.

52
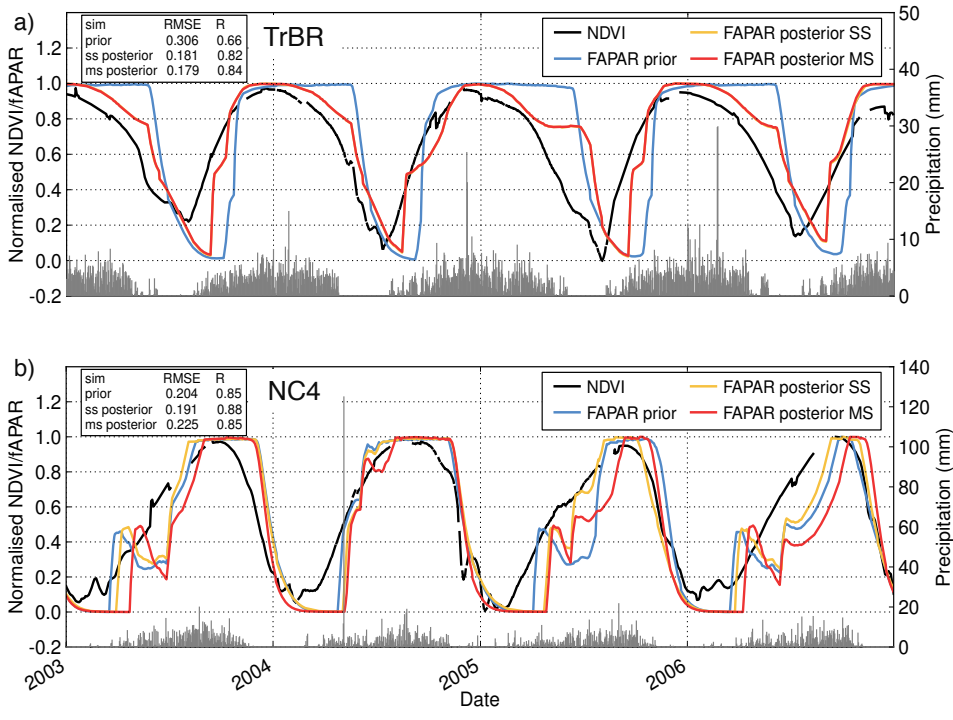
Figure 5: Example time-series (2002 – 2008 period) for the tropical deciduous PFTs for which phenology is driven by moisture availability. The two panels compare the normalized simulated fAPAR to the normalized MODIS NDVI (black curve) prior to (blue curve) and after the optimizations (orange curve = SS optimizations; red curve = MS optimization) for a a) TrBR tree site (5.77°S, 25.92°E) and a b) NC4 grass site (10.08°N, 4.32°W). The prior and posterior RMSE and R are given in the upper left boxes. The grey vertical lines show the daily precipitation.

53
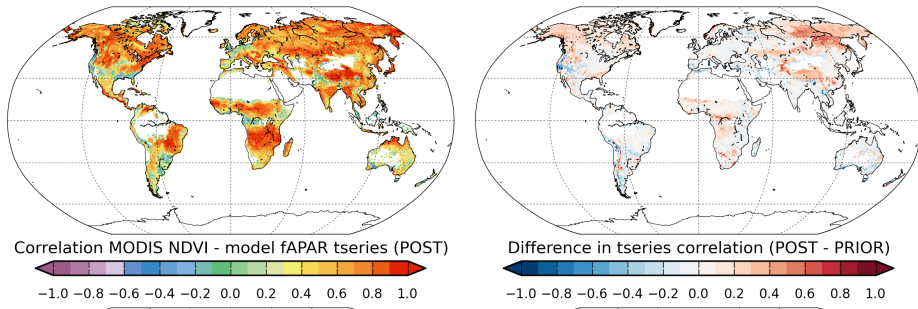
Figure 6: Global maps showing the correlation between the simulated fAPAR and MODIS NDVI data in the weekly time-series for the posterior simulation (left column) and the difference after optimization (posterior – prior) (right column). Note POST refers to the posterior simulation after optimization, and PRIOR to the simulation using the standard parameters of ORCHIDEE.

54
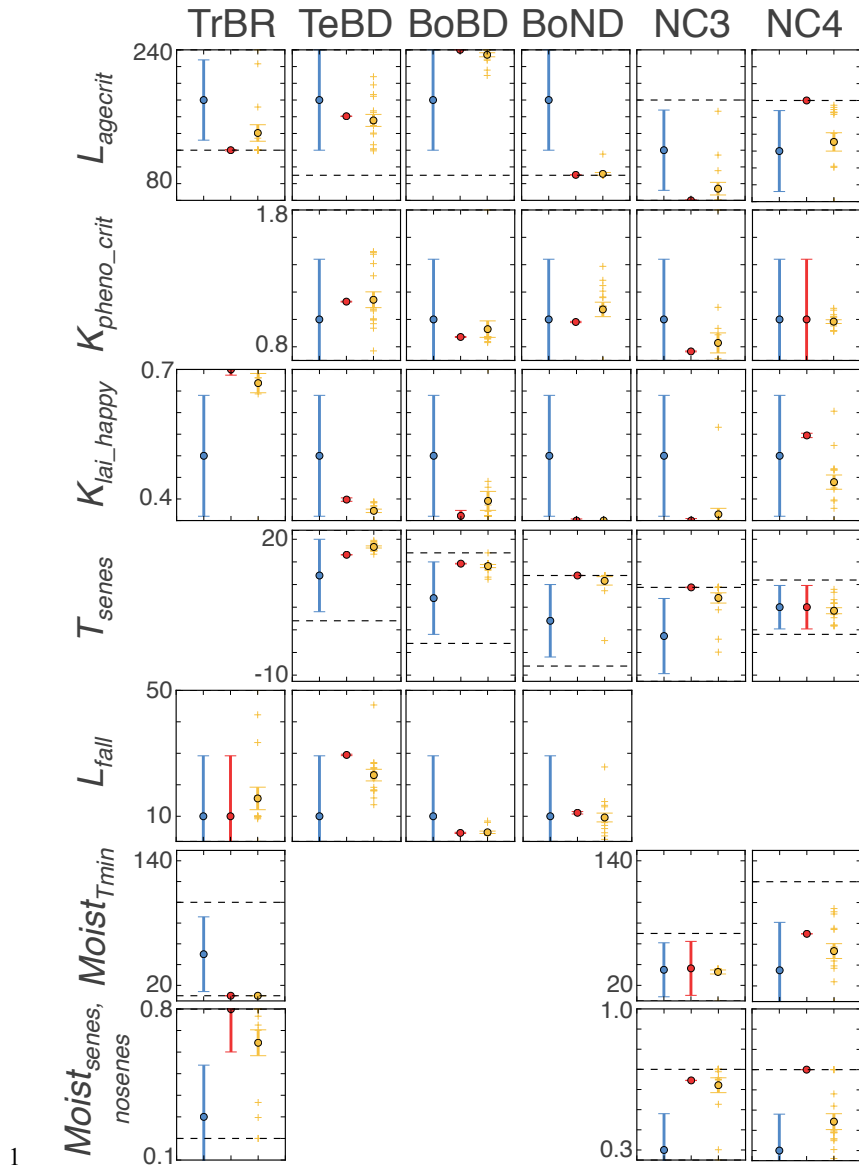
Figure 7: The prior (blue), MS posterior (red) and SS posterior (orange) parameter values (circles) and uncertainty (error bars – variance calculated in equation 3) for each parameter and each PFT. For the SS optimizations the circle and error bars represent the mean and standard error of the mean of all sites, and the crosses give the posterior values for each site.

Refer to Table 1 for a description of the PFTs and Figure 1 and Appendix A for a description of each parameter. The y-axis range represents the maximum upper and lower bounds for each parameter across all PFTs, and the horizontal dashed lines represent the parameter range for each individual PFT.

56
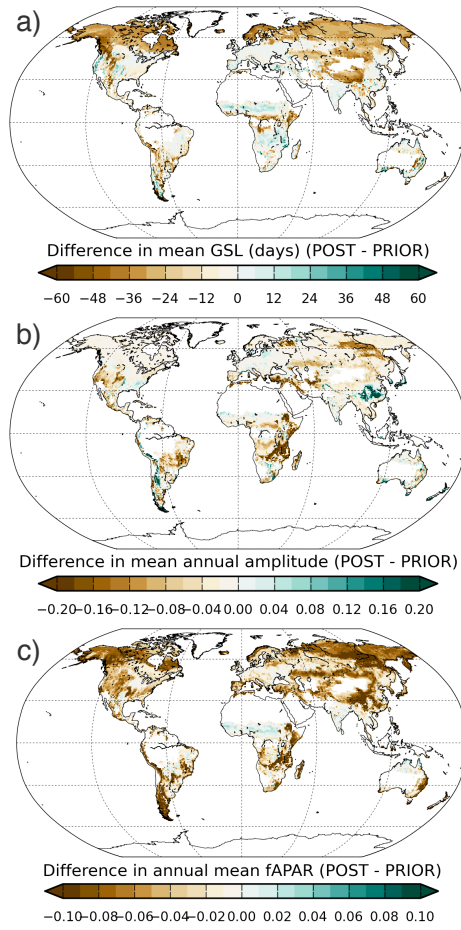
Figure 8: The difference (posterior – prior) of the simulated annual mean (over the 1990 – 2010 period) a) GSL (days); b) amplitude of the normalized fAPAR (range 0-1) and c) mean normalized fAPAR.

a)

Trend in fAPAR annual mean (1990 - 2010) (PRIOR)

−0.02   −0.01   0.00   0.01   0.02

b)

Trend in fAPAR annual mean (1990 - 2010) (POST)

−0.02   −0.01   0.00   0.01   0.02

c)

Difference in mean annual fAPAR trend (POST - PRIOR)

−0.010   −0.005   0.000   0.005   0.010
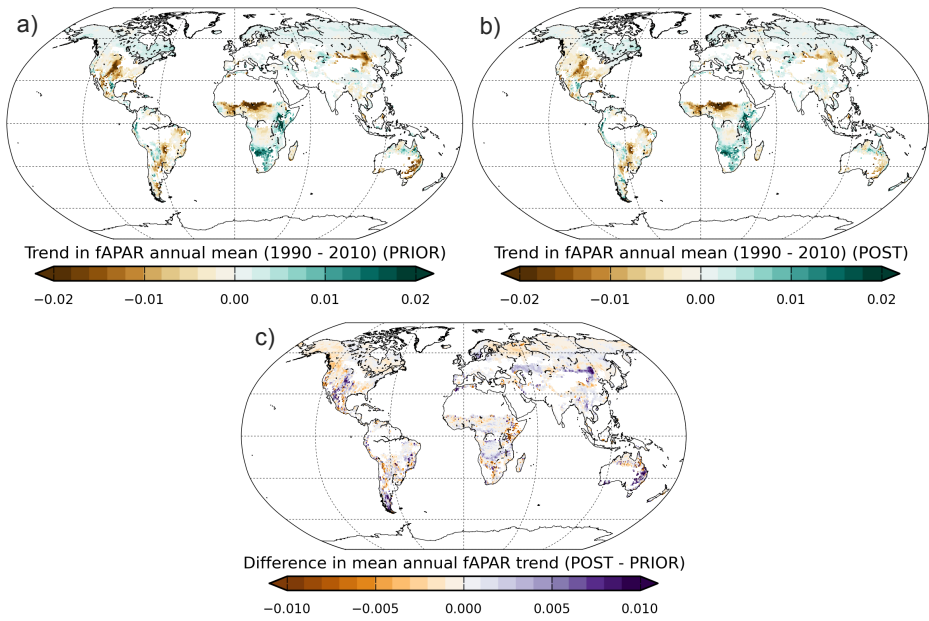
Figure 9: Linear trend (yr^{-1}) in the annual mean of the simulated normalized fAPAR for the 1990 – 2010 period: a) prior simulation; b) posterior simulation; c) difference between the prior and posterior (posterior – prior).

6   Supplementary Material
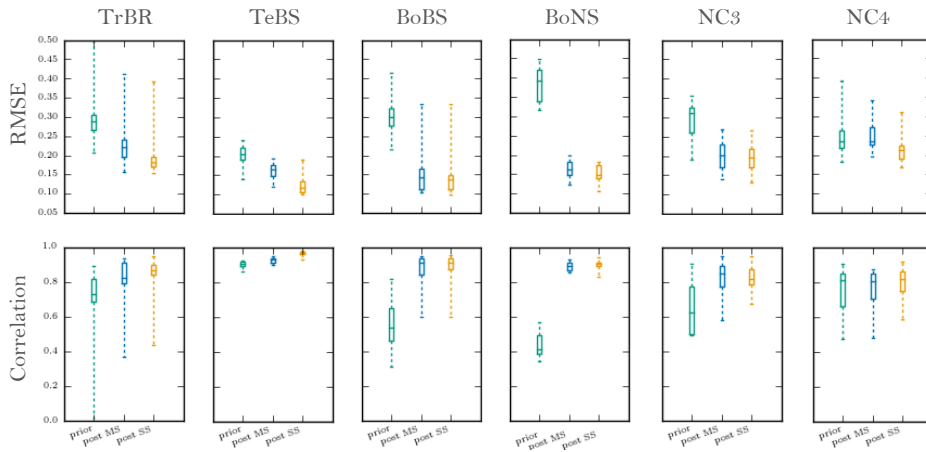
Figure S1. Box and whisker plots showing the spread in the prior and single-site (SS) and multi-site (MS) posterior RMSE and R between the normalized modeled fAPAR and MODIS NDVI data across all sites for all optimized PFTs. The middle line shows the median, the lower and upper edges of the box correspond to the 25th and 75th percentile respectively, and the range of the whiskers corresponds to the maximum and minimum RMSE and R.
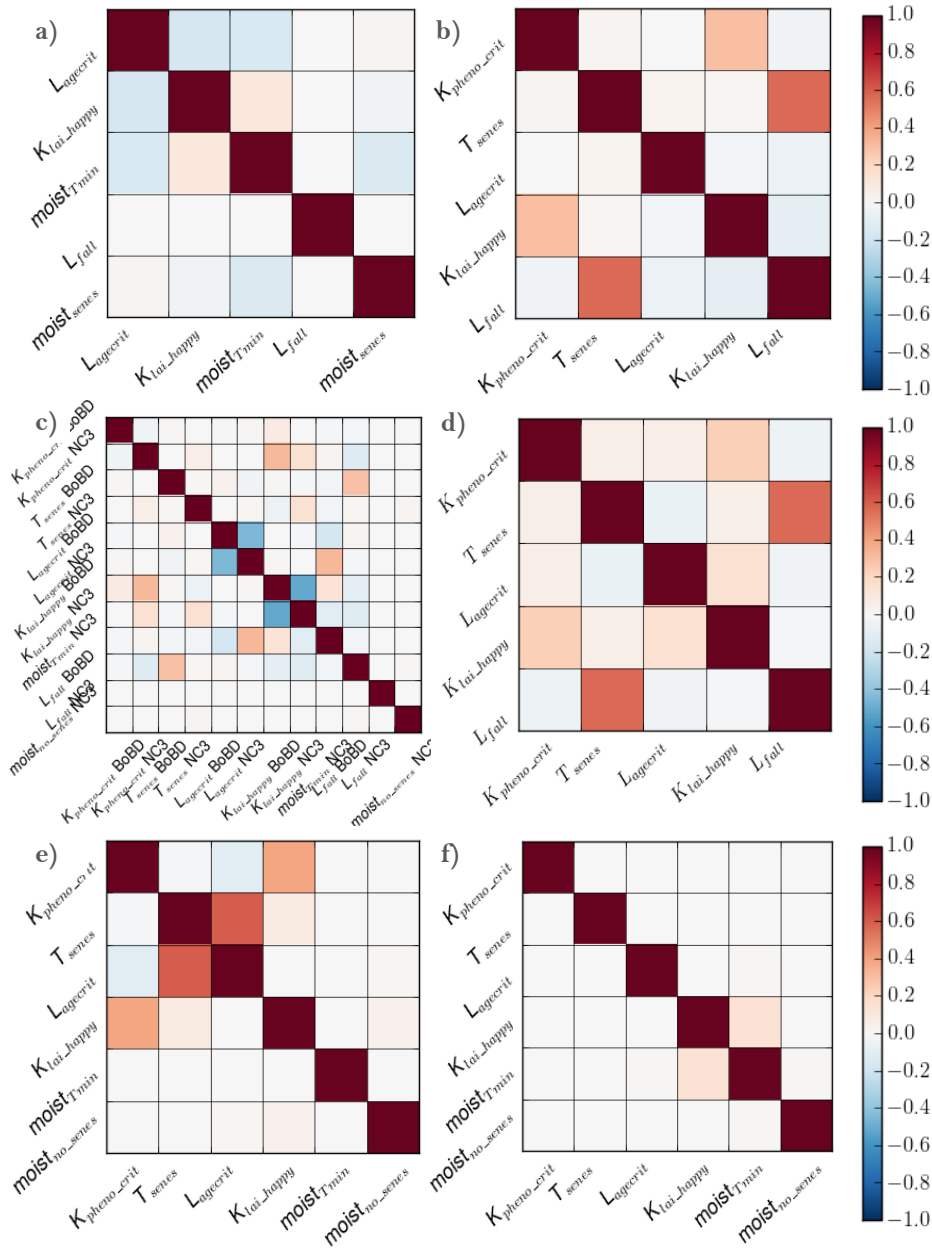
Figure S2. Parameter posterior covariance matrices for MS optimization for the a) TrBR; b) TeBD; c) BoBD; d) BoND; e) NC3; f) NC4 PFTs. Note in c) that BoBD sites contained

1 significant fraction of NC3 grasses and therefore the parameters were optimized for both

2 PFTs (see Section 3.3.3).

3

4

5